Assessment of evolving TRMM-based multisatellite real-time precipitation estimation methods and their impacts on hydrologic prediction in a high latitude basin

Bin Yong,[1,2] Yang Hong,[2] Li-Liang Ren,[1] Jonathan J. Gourley,[3] George J. Huffman,[4,5] Xi Chen,[1] Wen Wang,[1] and Sadiq I. Khan[2]

Received 27 October 2011; revised 5 March 2012; accepted 31 March 2012; published 5 May 2012.

[1] The real-time availability of satellite-derived precipitation estimates provides hydrologists an opportunity to improve current hydrologic prediction capability for medium to large river basins. Due to the availability of new satellite data and upgrades to the precipitation algorithms, the Tropical Rainfall Measuring Mission (TRMM) Multisatellite Precipitation Analysis real-time estimates (TMPA-RT) have been undergoing several important revisions over the past ten years. In this study, the changes of the relative accuracy and hydrologic potential of TMPA-RT estimates over its three major evolving periods were evaluated and inter-compared at daily, monthly and seasonal scales in the high-latitude Laohahe basin in China. Assessment results show that the performance of TMPA-RT in terms of precipitation estimation and streamflow simulation was significantly improved after 3 February 2005. Overestimation during winter months was noteworthy and consistent, which is suggested to be a consequence from interference of snow cover to the passive microwave retrievals. Rainfall estimated by the new version 6 of TMPA-RT starting from 1 October 2008 to present has higher correlations with independent gauge observations and tends to perform better in detecting rain compared to the prior periods, although it suffers larger mean error and relative bias. After a simple bias correction, this latest data set of TMPA-RT exhibited the best capability in capturing hydrologic response among the three tested periods. In summary, this study demonstrated that there is an increasing potential in the use of TMPA-RT in hydrologic streamflow simulations over its three algorithm upgrade periods, but still with significant challenges during the winter snowing events.

Citation: Yong, B., Y. Hong, L.-L. Ren, J. J. Gourley, G. J. Huffman, X. Chen, W. Wang, and S. I. Khan (2012), Assessment of evolving TRMM-based multisatellite real-time precipitation estimation methods and their impacts on hydrologic prediction in a high latitude basin, *J. Geophys. Res.*, *117*, D09108, doi:10.1029/2011JD017069.

1. Introduction

[2] Precipitation is fundamental to life on Earth, and it is among the most important factors in energy and mass fluxes that dominate the weather, climate, hydrology, and ecological systems. Therefore, precipitation measurements offer essential information in understanding the balance of the global energy and water cycle exchange that drives most hydrologic models and has direct impacts on the planetary circulation of the atmosphere [*Sorooshian*, 2004; *Ebert et al.*, 2007]. However, accurately measuring precipitation at regional or global scales has been a challenging task due to its high small-scale variability in space and time. Conventional rain gauge and meteorological radar networks have their own limitations because their distributions are often sparse and data availability in remote regions and in complex terrain is rather limited [*Griffith et al.*, 1978; *Simpson et al.*, 1996; *Astin*, 1997; *Vicente et al.*, 1998; *Huffman et al.*, 2001; *Margulis and Entekhabi*, 2001; *Maddox et al.*, 2002; *Steiner et al.*, 2003]. Thus, satellite-based precipitation estimates play an important role in detecting rainfall distribution and have been complementary to the ground-based rain gauge and radar measurements. Since the launch of the Tropical Rainfall Measuring Mission (TRMM) [*Simpson et al.*, 1988; *Kummerow et al.*, 2000] in 1997, there has been a growing number of real-time and quasi-global satellite precipitation products [*Sorooshian et al.*, 2000; *Joyce et al.*, 2004; *Hong*

[1]State Key Laboratory of Hydrology-Water Resources and Hydraulic Engineering, Hohai University, Nanjing, China.
[2]School of Civil Engineering and Environmental Sciences, University of Oklahoma, Norman, Oklahoma, USA.
[3]National Severe Storm Laboratory, NOAA, Norman, Oklahoma, USA.
[4]Science Systems and Applications, Inc., Lanham, Maryland, USA.
[5]Laboratory for Atmospheres, NASA Goddard Space Flight Center, Greenbelt, Maryland, USA.

Corresponding Author: Y. Hong, School of Civil Engineering and Environmental Sciences, University of Oklahoma, Norman, OK 73019, USA. (yanghong@ou.edu)

0148-0227/12/2011JD017069

Table 1. Time History of Major Upgrades of Microwave Satellites/Sensors Introduced Into the TMPA Processing[a]

Period	Satellites	Sensors	Period of Record	Nominal Coverage	Current Status
Period I	TRMM	TMI	8 Dec. 1997–Current	40° N-S	Active
	TRMM	PR	8 Dec. 1997–Current	38° N-S	Active
	DMSP-F13	SSM/I	29 Jan. 2002–18 Nov. 2009	85° N-S	Inactive
	DMSP-F14	SSM/I	29 Jan. 2002–23 Aug. 2008	85° N-S	Inactive
	DMSP-F15	SSM/I	29 Jan. 2002–14 Aug. 2006	85° N-S	Active, but unusable
Period II	Aqua	AMSR-E	3 Feb. 2005–Current	85° N-S	Active
	NOAA-15	AMSU-B	3 Feb. 2005–Current	Global	Active
	NOAA-16	AMSU-B	3 Feb. 2005–Current	Global	Active
	NOAA-17	AMSU-B	3 Feb. 2005–17 Dec. 2009	Global	Inactive
	NOAA-18	MHS	27 Nov. 2007–Current	Global	Active
Period III	MetOP-1	MHS	27 Mar. 2009–Current	Global	Active
	DMSP-F16	SSMIS	Being incorporated into TMPA	85° N-S	Active
	DMSP-F17	SSMIS	Being incorporated into TMPA	85° N-S	Active

[a]Notation: Except for above microwave satellites/sensors, the international constellation of geosynchronous-orbit meteorological satellites including the Geosynchronous Operational Environmental Satellites (GOES, United States), the Geosynchronous Meteorological Satellite (GMS, Japan), and the Meteorological Satellite (Meteosat, European Community) provide the infrared (IR) data on a 4 km-equivalent grid over the latitude band 60° N-S for TMPA-RT.

et al., 2004; *Turk and Miller*, 2005; *Huffman et al.*, 2007; *Kubota et al.*, 2007] for a variety of scientific uses and natural hazard detection and warning, such as flood forecasting, drought assistance, landslide detection, and water quality monitoring. The planned Global Precipitation Measurement (GPM) mission with an approaching launch date of 14 February 2014 [*Tapiador et al.*, 2012], which will use an international constellation of microwave sensors, is anticipated to provide more accurate global precipitation products so as to improve our scientific understanding of the Earth system from space [*Smith et al.*, 2007; *Hou*, 2008]. As a prelude to GPM, the current operational TRMM Multisatellite Precipitation Analysis (TMPA) is intended to provide the best estimates of quasi-global precipitation [*Huffman et al.*, 2007]. The TMPA merged data collected by two different types of satellite sensors: low-Earth orbiting passive microwave (PMW) data, which have a direct physical connection to the hydrometeor profiles but sparse sampling of the time-space occurrence of precipitation, and geostationary infrared (IR) data with excellent space-time coverage (approximately 30 min/4 $\times$ 4 km), but indirect physical relations with precipitation. The standard TMPA products include real time (3B42 RT, hereafter referred to as TMPA-RT) and post-real time research products (3B42 V6, hereafter referred to as TMPA-V6), and both versions of the TMPA products have been provided for a sufficiently long time that researchers have had the chances to develop and start reporting on various applications and validation studies that employ one or both versions [*Huffman et al.*, 2010].

[3] Many prior studies have reported on the improvement of the TMPA-V6 products over TMPA-RT products through bias correction using monthly rain gauge accumulations [e.g., *Tian et al.*, 2007; *Su et al.*, 2008; *Li et al.*, 2009; *Dinku et al.*, 2010; *Gourley et al.*, 2010; *Hirpa et al.*, 2010; *Tobin and Bennett*, 2010; *Behrangi et al.*, 2011; *Bitew and Gebremichael*, 2011; *Yong et al.*, 2010; *Su et al.*, 2011]. However, it is the near real-time availability of the TMPA-RT products and high spatial (0.25° $\times$ 0.25°) and temporal (3h) resolution that has made them very attractive to the water resources community, especially in developing countries, in order to provide hydrologic predictions from which actions can be taken on medium to large river basins. Presently, TMPA-RT products have been widely utilized in a variety of research and operational applications [e.g., *Gottschalck et al.*, 2005; *Li et al.*, 2009; *Yong et al.*, 2010; *Tobin and Bennett*, 2010; *Behrangi et al.*, 2011; *Khan et al.*, 2011; *Romilly and Gebremichael*, 2011; *Su et al.*, 2011; *Wang et al.*, 2011]. For example, currently the global real-time flood monitoring system developed by NASA TRMM group (http://trmm.gsfc.nasa.gov/) [*Hong et al.*, 2007; *Wang et al.*, 2011; *Wu et al.*, 2012] has demonstrated the initial capability of using satellite-derived precipitation data as forcing for global river forecast models.

[4] During the course of TMPA-RT development, precipitation estimates from new sensors on various satellites were integrated and thus the real-time algorithm has undergone several updates. Table 1 summarizes all precipitation-sensing microwave satellites/sensors that were introduced into the TMPA processing at different historical periods. Generally speaking, the evolution of TMPA-RT can be separated into the following three main development periods: 29 January 2002 to 3 February 2005 (Period I), 3 February 2005 to 1 October 2008 (Period II), and 1 October 2008 to present (Period III). Specific details regarding the sensors used, nominal coverage, and algorithmic changes are provided in Appendix A.

[5] Given the dynamical evolution of the TMPA-RT algorithm by the Appendix A, a thorough understanding to the above mentioned major upgrades is critical to physically analyzing the changes of data accuracy and hydrologic potential of the real-time TMPA products across the three different developing periods. Many efforts have been made in prior studies to evaluate the hydrologic utility of TMPA-RT for different basins throughout the globe [e.g., *Li et al.*, 2009; *Dinku et al.*, 2010; *Hirpa et al.*, 2010; *Bitew and Gebremichael*, 2011; *Khan et al.*, 2011; *Su et al.*, 2011]. Yet, their study areas are rarely located at the high latitude bands beyond the current TMI/PR orbiting regions. Below, we highlight a number of questions about the TMPA-RT algorithm evolution with the intention of addressing them in this study: (1) Have the TMPA-RT estimates been significantly improved over the three major evolution periods? (2) TMI and TCI, the calibrators of TMPA-RT, provide

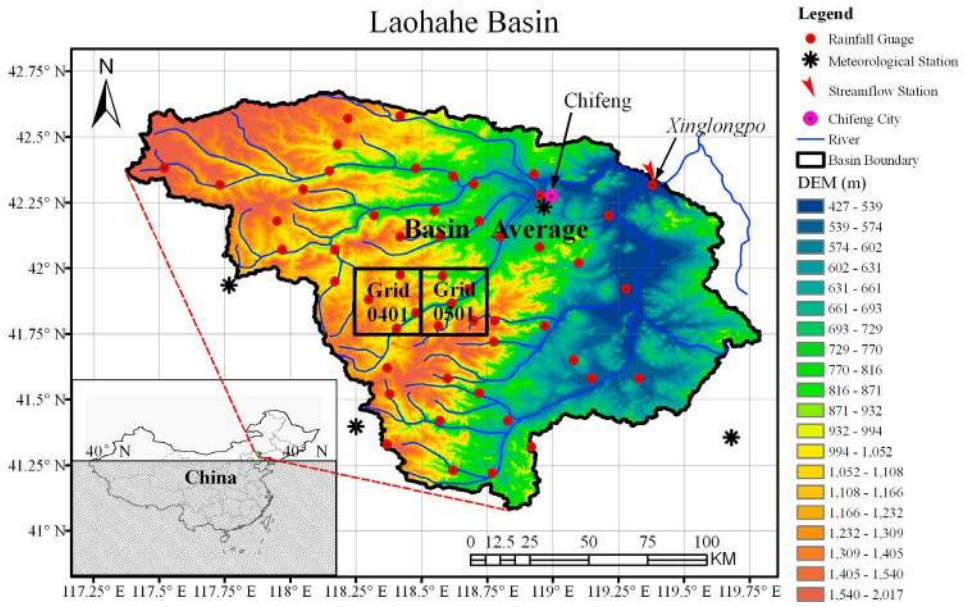

Figure 1. Map of Laohahe Basin situated beyond the TMI/PR orbiting bands (40°NS) and locations of rain gauges, meteorological stations, and streamflow station included in the study. Hydrologic evaluation of TMPA-RT during three major evolving periods was performed over the whole basin (i.e., Basin Average) and two selected 0.25° × 0.25°grids with black squares (i.e., Grid0501 and Grid0401), which contain 5 and 4 rain gauges, respectively.

coverage from 40°N-S. Thus, do the data of TMPA-RT that cover higher latitude bands beyond 40°suffer from large bias, especially in basins with snow covered land surfaces? (3) Are the latest TMPA-RT products (i.e., 3B42RT-Version6) much more similar to the gauge-adjusted TMPA-V6 estimates than the previous two periods as suggested by the developers, particularly in high-latitude basins? (4) Finally, how did changes in input data and algorithm design for TMPA-RT over the three different periods impact hydrologic prediction skill?

[6] *Yong et al.* [2010] evaluated the data accuracy and hydrological potential of TMPA-RT and TMPA-V6 in the Laohahe Basin, China within the TMPA latitude band (50°NS) but beyond the latitude band of the TMPA calibrator (40°N-S). In this study, we extend the work of *Yong et al.* [2010] by specifically addressing the above questions through evaluation of TMPA-RT precipitation products using independent gauge reports and examination of TMPA-RT estimates on hydrologic simulation using the three-layer Variable Infiltration Capacity (VIC-3L) Model [*Liang et al.*, 1994, 1996]. Section 2 describes the Laohahe basin, the data sets used, and the statistics used to evaluate TMPA precipitation estimates and resulting hydrologic simulations. The precipitation evaluation is divided into daily, monthly, and seasonal analyses in section 3; this section also evaluates the similarity between TMPA-RT to TMPA-V6. The impact of the algorithmic changes on hydrologic simulation is evaluated in section 4, and the paper is closed in section 5 with conclusions and future recommendations.

2. Study Basin, Observed Data and Methodology

[7] The Laohahe basin, of which a detailed description is provided in *Yong et al.* [2010], is located within the Chinese typical arid and semi-arid regions. Accurate precipitation estimates at high spatiotemporal scale is of particular importance for such drought-prone basins with heterogeneous distributions of surface water resources. Compared to other basins in the northern part of China, the Laohahe basin has a remarkably dense observation network that can offer detailed ground verification for the satellite-derived precipitation estimates (Figure 1). There are 52 rain gauges evenly distributed within this 18,112 km^2 basin and a streamflow station of Xinlongpo located at the watershed outlet to record observations of daily precipitation and streamflow continuously from January 1990 to September 2010. Both the China Meteorological Administration (CMA) and the Chinese Ministry of Water Resources (CMWR) operate all rain gauge networks over mainland China. In practice, the local workers record the precipitation using two approaches (i.e., tipping-bucket rain gauge and manual traditional ombrometer). Then these two types of recorded data are cross-checked and the final errors have to be controlled within 4% for daily rainfall observation according to the ministerial standard. Hence, the Laohahe basin gauge network is of high quality and is independent from what *Huffman et al.* [2007] used for the gauge correction of TMPA post-real-time products. With respect to snow observations, they introduced a known volume of warm water to thaw the snow in the standard vessel. So the liquid equivalency of the snow is computed as the total water volume minus the input warm water volume. The observers make a particular mark after the snow water equivalent digit in order to distinguish snow or rainfall as the precipitation type. Such manual but effective recording techniques can ensure the data quality and information of observed snow for our study. Ultimately, these precipitation data will be collected and edited in the Chinese Hydrology Almanac at the end of every year.

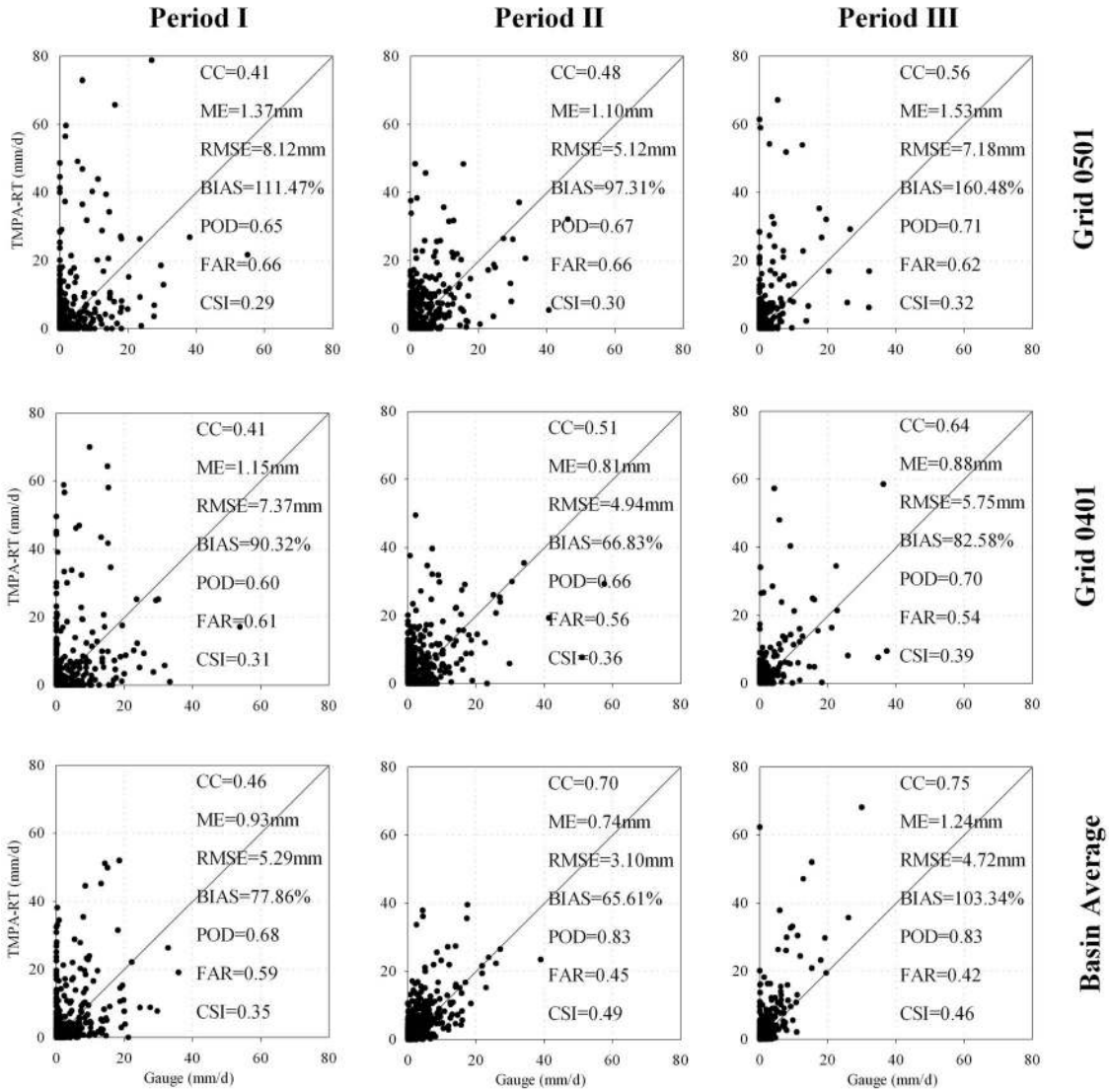

Figure 2. Scatterplots of the daily TMPA-RT versus gauge observation for (top row) Grid 0501, (middle row) Grid 0401, and (bottom row) Basin Average at (left column) period I, (middle column) period II, and (right column) period III.

[8] Daily maximum and minimum temperature and daily average wind speed from 1990 to 2010 were gathered from four meteorological stations to force the hydrologic model (see Figure 1). Other data sources such as a digital elevation model (DEM), soil surveys, and vegetation, which are needed to run the VIC-3L model, were taken from *Yong et al.* [2010]. The grid mesh size of the hydrologic model used in this study is $\frac{1}{16}^\circ \times \frac{1}{16}^\circ$. To quantify the accuracy of satellite-derived precipitation estimates, we used three types of statistical indices including Pearson linear correlation coefficient (CC), mean error (ME), root mean squared error (RMSE), relative bias (BIAS), and contingency table-based detection of rainy events (i.e., probability of detection (POD), false alarm rate (FAR), and critical success index (CSI)). In addition, Nash-Sutcliffe Coefficient of Efficiency (NSCE) was used to assess the hydrologic model fit between simulated and observed streamflow. The interested reader can refer to all above statistical indices for their corresponding formulae and meaning in Table 1 in *Yong et al.* [2010].

3. Evaluation and Comparison of Satellite Precipitation Estimates

[9] Our evaluation and comparison were performed over three domains including two selected $0.25^\circ \times 0.25^\circ$ grids (hereafter labeled as "Grid0501" and "Grid0401"; see Figure 1) corresponding to TRMM pixel resolution as well as the basin-averaged analysis (hereafter referred to as "Basin Average"). The two, nested grid locations were chosen because they contain 4–5 rain gauges within them and provide an analysis at the fine, TRMM pixel scale. Furthermore, there are significant differences in terrain and land cover between these two grids though they are adjacent to each other. Almost 80% of Grid0401 is at high elevation (>1000 m) with evergreen broadleaf or coniferous trees,

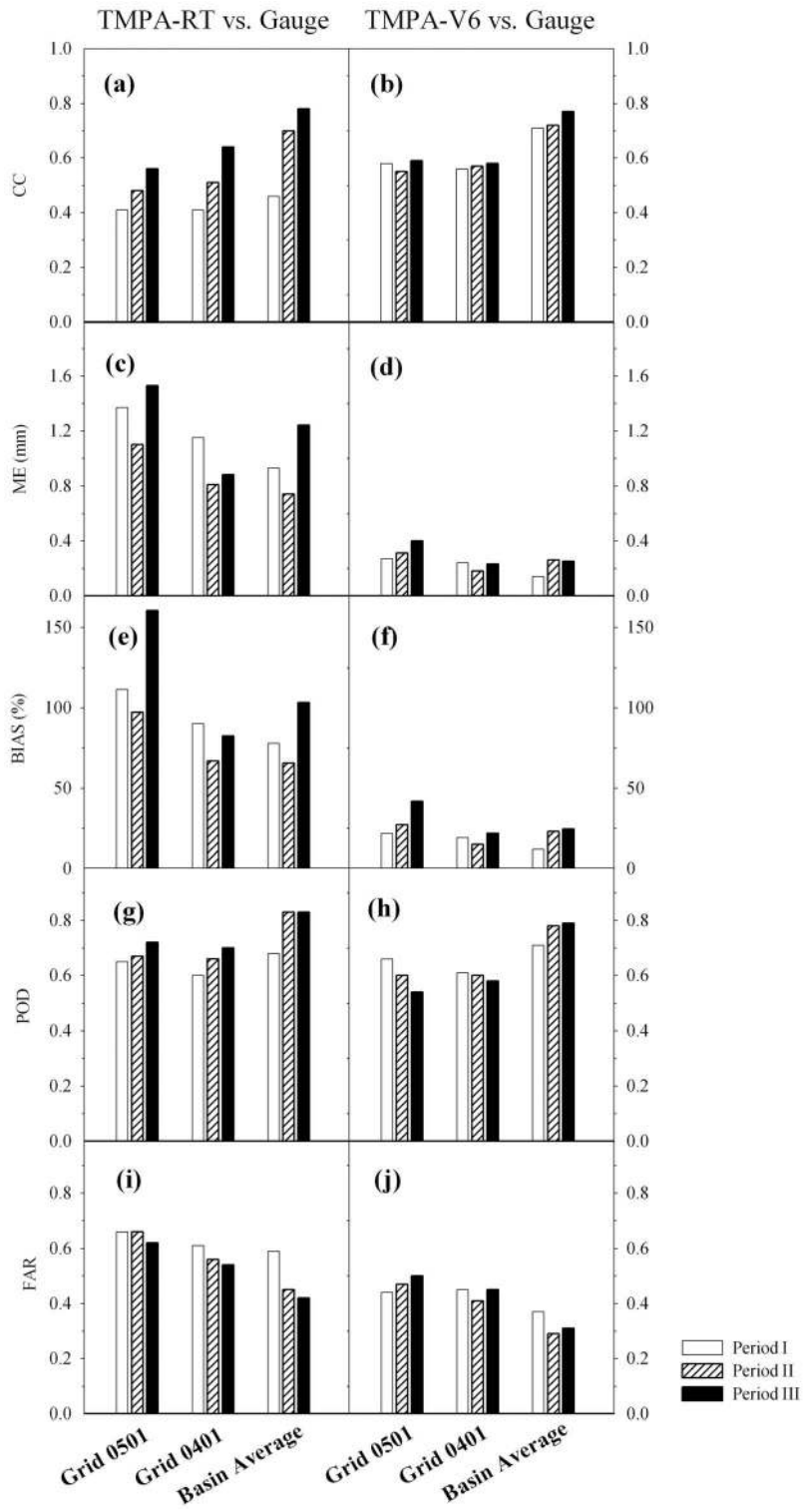

Figure 3. Comparisons of statistical indices of the daily (left) TMPA-RT and (right) TMPA-V6 versus gauge observation at three evolving periods (I-III): (a and b) correlation coefficient, (c and d) mean error, and (e and f) relative bias, (g and h) probability of detection, (i and j) false alarm ratio.

while most regions within Grid0501 are considered flat croplands and lowlands (elevations <1000 m) and are predominately covered by sparse grassland and shrubs. The rain gauge accumulations from each gauge are averaged within each TRMM pixel so that they can be compared to the TMPA estimates. The objective aims to investigate the evolution of the performance of TMPA-RT during the three periods at daily, monthly, and seasonal time scale. Algorithm skill in estimating rainfall amounts is compared to that obtained with TMPA-V6 in order to assess whether TMPA-RT is

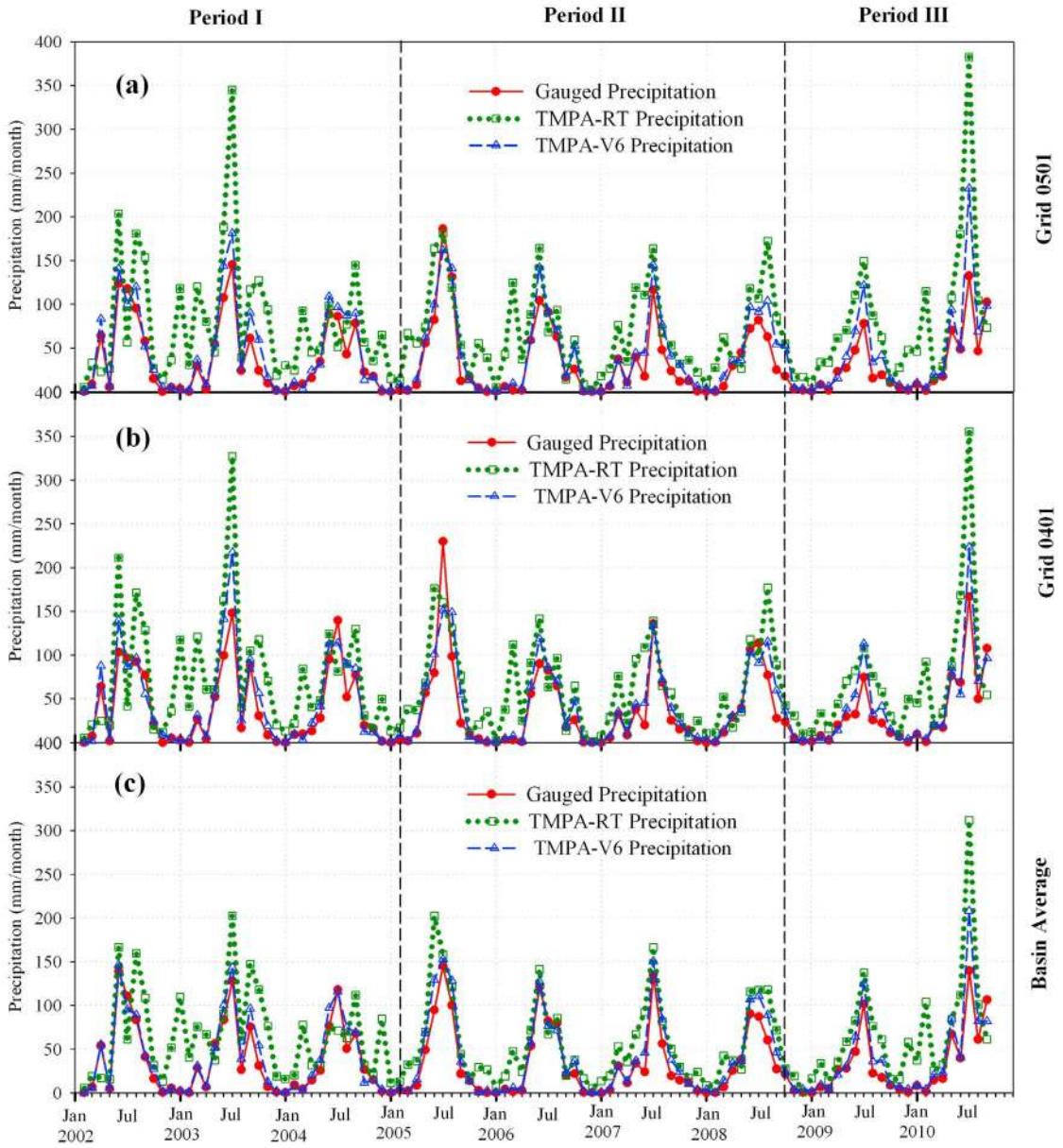

Figure 4. Monthly variations of gauged precipitation, TMPA-RT, and TMPA-V6 during three evolving periods, i.e., Period I (Feb. 2002–Jan. 2005), Period II (Feb. 2005–Sep. 2008), and Period III (Oct. 2008–Sep. 2010): (a) Grid 0501, (b) Grid 0401, and (c) Basin Average.

approaching the skill of TMPA-V6 following the critical algorithm updates. Considering both the major upgrade periods of TMPA-RT and the time span of available observation data in the Laohahe basin, we separated the comparison periods of this study into three parts: Period I (1 February 2002–1 January 2005), Period II (1 February 2005–30 September 2008), and Period III (1 October 2008–30 September 2010). The different sensors, data inputs, and algorithm changes during these three time periods are summarized in Table 1 and the details are available in the Appendix A.

3.1. Daily Comparison

[10] We start with the evaluation of daily TMPA-RT against averaged rain gauge observations over Grid0501, Grid0401, and Basin Average across Periods I, II, III, respectively (Figures 2 and 3). There is a gradually increasing CC between TMPA-RT and observed precipitation from Period I to III for all three domains (Figure 3a). Taking the domain of Basin Average for example, the CC value increases from 0.46 in Period I to 0.75 in Period III (increasing by approximately 63%). With respect to ME and BIAS, TMPA-RT during Period III, however, didn't perform as well as expected, and was even worse than Period I for Grid 0501 and Basin Average (Figures 3c and 3e). But, it is worth noting that TMPA-RT exhibits a significant improvement in the skill of detecting rain events. The indices of POD and CSI are substantially increased throughout the three evolving periods (Figures 2 and 3g), while the FAR has an obvious decreasing tendency (Figure 3i). The results

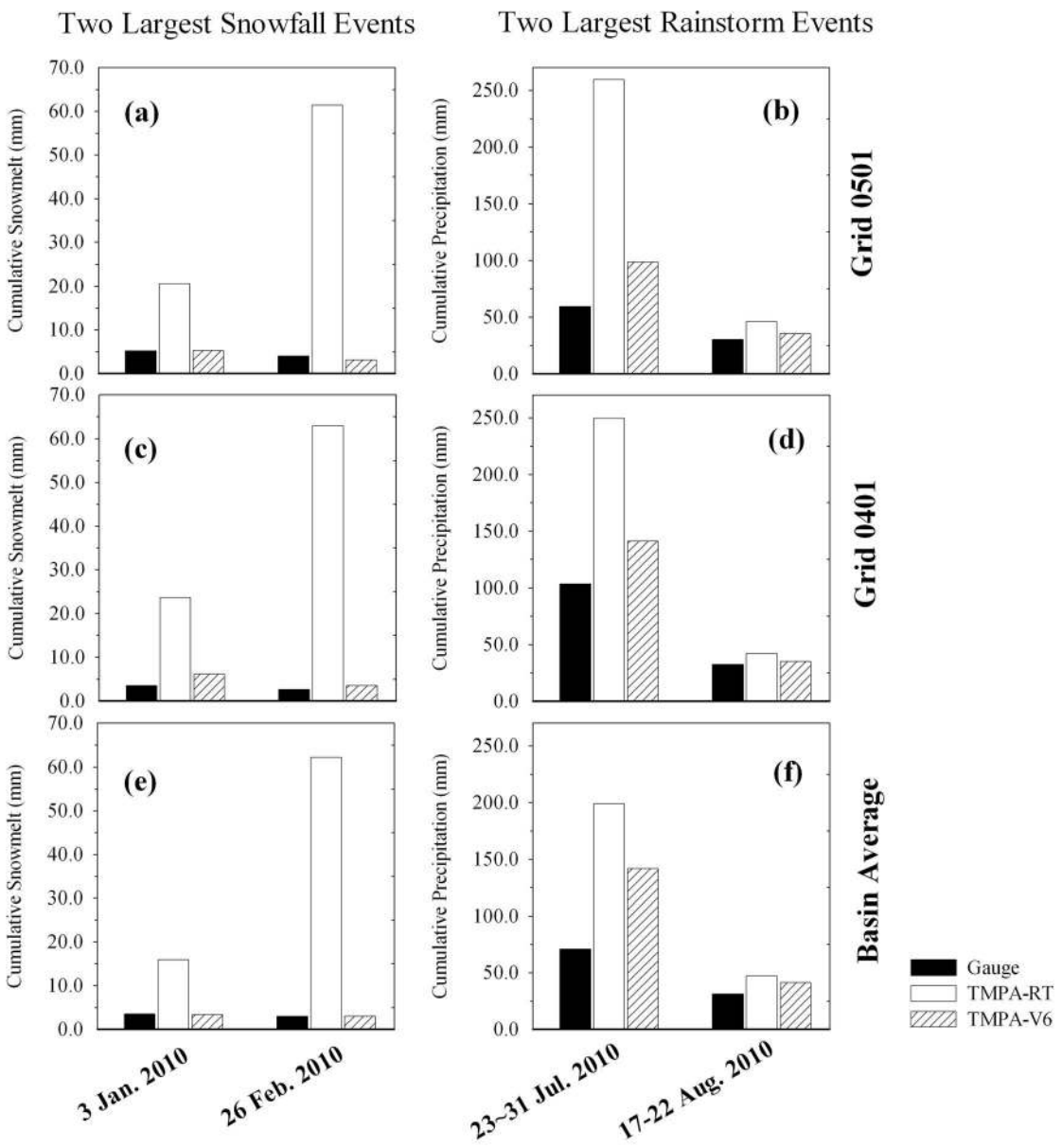

Figure 5. Comparisons of gauge observation, TMPA-RT, and TMPA-V6 for two largest snowfall events (i.e., 3 Jan. and 26 Feb.) in the winter of 2010 and two heavy rainstorms (i.e., 23–31 Jul. and 17–22 Aug.) in the summer of 2010: (a and b) Grid 0501, (c and d) Grid 0401, and (e and f) Basin Average.

suggest that the new algorithm adjustments to 3B42RT-Version6 (i.e., TMPA-RT during Period III) do not always reduce the error and bias of the 3B42RT estimates, but they apparently provide higher correlation with gauge observations and better detection for precipitation events in high-latitude basins, which are potentially favorable factors for improving the hydrologic potential of TMPA-RT. On the other hand, statistics describing TMPA-V6 performance don't reflect the same tendencies noted with TMPA-RT over the three periods, though it has relatively low ME and BIAS (see the right column of Figure 3). Last, scatterplots in Figure 2 reveal an interesting phenomenon in that TMPA-RT has a slight tendency to overestimate lower rainfall rates and underestimate higher ones, which is a similar finding in an evaluation of GOES-based rainfall estimates from *Vicente et al.* [1998].

3.2. Monthly Comparison

[11] To directly assess the skill of the TMPA products in tracking the monthly variation of precipitation over the three tested periods, we compare the time series of TMPA-RT, TMPA-V6, and gauge observations over Grid 0501, Grid 0401, and Basin Average in Figure 4. Similar to the daily results, the purely satellite-derived TMPA-RT demonstrated a relatively poor performance in tracing the monthly variations of precipitation during Period I, while substantial improvements were realized after 2005. This result confirms the assertion of *Huffman et al.* [2010] that all TMPA-RT

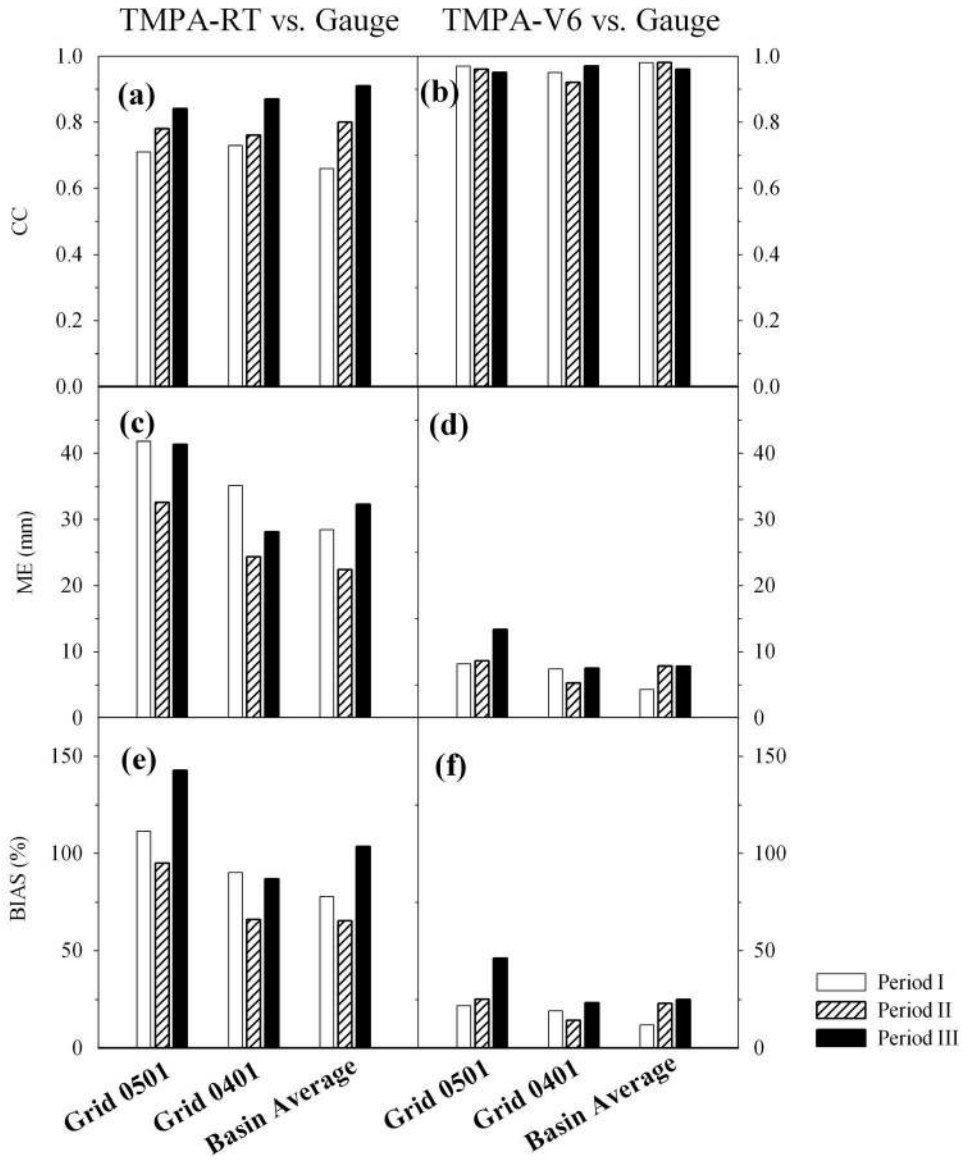

Figure 6. Same as Figure 3 but for monthly precipitation: (a and b) correlation coefficient, (c and d) mean error, and (e and f) relative bias.

data sets produced before 3 February 2005 should not be used. However, at least in this high-latitude study basin, the TMPA-RT estimates after 2005 still overestimate precipitation compared to gauges, especially during the winter and summer months. The BIAS of TMPA-RT during Period III is even larger than that during Period II. But the monthly CC of Period III looks better than the prior two periods. We further analyzed the TMPA-RT estimates for two largest snowfall events in the winter of 2010 and two heavy rainstorms in the summer of 2010 (see Figure 5). TMPA-RT significantly overestimates precipitation during all these extreme weather events. For example, for the snowfall event that occurred on 26th February 2010, TMPA-RT dramatically overestimated gauge observations over the whole basin by approximately 2000% (i.e., 62.24 mm for TMPA-RT versus 2.96 mm by gauges for Basin Average). Similarly, for the largest rainstorm in 2010, the cumulative gauge precipitation from the 23rd to 31st July is 70.81mm for Basin Average, while the corresponding estimation of TMPA-RT is 198.81mm, indicating overestimation of 180%. In contrast, precipitation from TMPA-V6 remains in good agreement with gauge precipitation throughout all the periods (see Figures 4 and 5).

[12] Next, we selected three statistical indices, CC, ME, and BIAS to illustrate the evolution of monthly error characteristics of TMPA-RT and TMPA-V6. The values of CC improve throughout all three tested periods, while relatively large values of ME and BIAS were still found for Period III (see Figure 6). Above analyses suggest that the incorporation of AMSU-B and AMSR-E on February 2005, which provides more passive microwave data covering high-latitude bands, significantly improved the accuracy of TMPA-RT precipitation estimates. Another important factor might be that the microwave-calibrated IR coefficients were updated

Table 2. Statistical Summary of the Seasonal Comparison of Daily TMPA-RT Versus Gauge at Three Evolving Periods[a]

Index	Evaluating Domains	Spring			Summer			Autumn			Winter (Winter but Excluding Snowing Days)		
		Period I	Period II	Period III	Period I	Period II	Period III	Period I	Period II	Period III	Period I	Period II	Period III
CC	Grid 0501	0.16	0.47	0.63	0.38	0.47	0.68	0.36	0.39	0.53	0.02 [0.03]	0.03 [0.08]	0.15 [0.45]
	Grid 0401	0.16	0.49	0.65	0.37	0.48	0.72	0.36	0.49	0.56	0.003 [0.02]	0.08 [0.15]	0.12 [0.47]
	Basin Average	0.16	0.60	0.69	0.48	0.68	0.85	0.39	0.65	0.86	0.05 [0.08]	0.14 [0.23]	0.15 [0.49]
ME (mm)	Grid 0501	1.05	1.38	0.90	1.48	1.29	3.51	1.77	0.97	0.31	1.19 [0.55]	0.64 [0.35]	1.39 [0.41]
	Grid 0401	1.00	1.04	0.59	1.47	0.84	2.47	1.04	0.75	0.18	1.09 [0.53]	0.55 [0.39]	1.24 [0.38]
	Basin Average	0.62	0.76	0.51	0.49	1.07	2.33	1.39	0.60	0.82	1.24 [0.56]	0.44 [0.30]	1.29 [0.45]
RMSE (mm)	Grid 0501	6.00	4.39	4.28	12.28	7.79	11.89	7.77	3.72	3.45	3.98 [1.89]	2.13 [1.28]	5.80 [1.64]
	Grid 0401	6.14	4.07	4.33	11.32	7.70	9.90	5.94	3.49	3.66	3.90 [2.09]	1.83 [1.25]	5.70 [1.60]
	Basin Average	4.60	2.38	2.65	6.62	4.99	6.59	5.45	1.83	2.72	4.11 [1.85]	1.40 [0.83]	5.60 [1.66]
BIAS (%)	Grid 0501	130.19	173.76	109.54	49.24	44.95	175.56	169.90	199.43	35.29	2104.65 [1086.49]	1399.94 [751.89]	1230.79 [341.39]
	Grid 0401	134.89	133.91	66.29	48.32	26.61	108.80	84.60	141.65	18.61	1640.58 [844.06]	1357.14 [1070.02]	1096.01 [317.32]
	Basin Average	85.39	106.35	59.09	46.52	36.71	106.58	135.06	118.10	35.89	1742.62 [835.71]	940.51 [707.14]	1300.39 [449.65]
POD	Grid 0501	0.54	0.69	0.57	0.61	0.72	0.79	0.88	0.54	0.54	0.36 [0.37]	0.33 [0.33]	0.20 [0.20]
	Grid 0401	0.50	0.61	0.54	0.60	0.71	0.81	0.74	0.60	0.64	0.20 [0.21]	0.25 [0.33]	0.50 [0.50]
	Basin Average	0.56	0.77	0.64	0.66	0.86	0.92	0.84	0.83	0.90	0.50 [0.33]	0.33 [0.50]	0.33 [0.33]
FAR	Grid 0501	0.84	0.82	0.69	0.36	0.38	0.37	0.60	0.69	0.68	0.94 [0.95]	0.98 [0.96]	0.97 [0.95]
	Grid 0401	0.75	0.75	0.55	0.37	0.30	0.44	0.55	0.59	0.64	0.98 [0.98]	0.97 [0.97]	0.89 [0.85]
	Basin Average	0.75	0.63	0.55	0.37	0.21	0.23	0.54	0.54	0.60	0.96 [0.97]	0.97 [0.96]	0.97 [0.95]
CSI	Grid 0501	0.14	0.16	0.25	0.46	0.50	0.54	0.38	0.24	0.25	0.06 [0.05]	0.02 [0.03]	0.03 [0.04]
	Grid 0401	0.20	0.22	0.33	0.45	0.55	0.49	0.39	0.32	0.30	0.02 [0.02]	0.03 [0.03]	0.10 [0.15]
	Basin Average	0.21	0.33	0.36	0.48	0.70	0.72	0.43	0.42	0.38	0.04 [0.03]	0.03 [0.04]	0.03 [0.04]
Error Contribution (EC)		20.73%			45.28%			18.94%			15.05%		

[a]Notation: The seasonal comparison includes five cases: spring [March–May (MAM)], summer [June–August (JJA)], autumn [September–November (SON)], winter [December–February (DJF)], and winter but excluding snowing days. The computing equation of Error Contribution (EC) is defined as: $EC = \frac{\sum_{i=1}^{n} |S_i - G_i|}{\sum_{j=1}^{m} |S_j - G_j|} \times 100\%$, among which S_i and G_i are satellite precipitation and gauged observation, and n and m represent the number of a certain season and all season days, respectively.

Table 3. Number of Snowing Days, Observed Cumulative Snowmelt, and Statistical Indices (CC, ME, RMSE, and BIAS) of Daily TMPA-RT and TMPA-V6 Versus Gauge for Every Winter From 2005 to 2010 in Laohahe Basin[a]

Phases	Year	Number of Snowing Days	Observed Cumulative Snowmelt	TMPA-RT Versus Gauge				TMPA-V6 Versus Gauge				Performance Level
				CC	ME	RMSE	BIAS	CC	ME	RMSE	BIAS	
Period II	2005	4	5.434	0.086	1.153	3.825	1909.40%	0.120	0.052	0.443	85.63%	Poor
	2006	4	4.766	−0.042	0.537	1.593	1013.50%	−0.009	0.014	0.381	26.56%	Average
	2007	2	3.400	0.249	0.388	1.232	1023.75%	0.539	0.029	0.273	75.19%	Average
	2008	3	3.480	0.237	0.409	1.319	1497.97%	0.218	0.061	0.393	221.84%	Average
Period III	2009	2	2.350	0.773	0.489	1.679	597.42%	0.888	0.085	0.313	104.31%	Good
	2010	5	10.540	−0.042	2.099	7.733	1791.94%	−0.045	0.076	0.857	64.99%	Poor

[a]Notation: If the snowing observations of more than half rain gauges distributed within the whole basin exceed the threshold of 0.1mm, this day will be labeled as a "snowing day."

every 3hr instead of each pentad, and thus the IR-based scheme for filling PMW coverage gaps was substantially changed at higher latitudes. Relative to the prior two periods, the latest upgrades of TMPA-RT greatly helped it to improve its correlation with observed precipitation and improve the skill of detecting rainy events, but the incorporation of PMW and IR data did little to reduce ME and BIAS. We speculate that the causes for such large bias of the current TMPA-RT version come from two sources: 1) The PMW data for TMPA are first calibrated by the TRMM Combined Instrument (TCI) estimate, which combines data from TMI and PR. However, the coverage of both TMI and PR is limited within the latitude bands between 40°N-S. 2) Likewise, the TMI-TCI used as the climatological monthly calibrator in 3B42RT-Version6 also cannot cover latitude bands beyond 40°. Thus, the IR-based schemes are poorly calibrated for higher latitudes to the passive microwave, especially during the cool season. Therefore, the upgrades to the TMPA algorithm had little impact on ME and BIAS. The monthly TMPA-V6 data didn't reveal any clear trends in error characteristics over the three periods, thus the relatively higher CC and lower ME can mostly be attributed to the monthly gauge adjustments yielding the post-real-time products [*Su et al.*, 2008; *Yong et al.*, 2010].

3.3. Seasonal Comparison

[13] Table 2 lists the statistical summary of seasonal comparisons including spring [March–May (MAM)], summer [June–August (JJA)], autumn [September–November (SON)], and winter [December–February (DJF)]. We also specifically computed the statistics during winter by separating snow versus rain events in order to assess the impact of precipitation phase on TMPA-RT. Generally, there are strong seasonal variations in the computed statistics during the three tested periods. All evaluations over Grid0501, Grid0401, and Basin Average show higher CC, POD, and CSI and lower FAR in the summer compared to other seasons, while the worst performance occurs in winter. In terms of the first four indicators, all seasons tended to experience better precipitation estimates during the three evolving periods of TMPA-RT. For example, the CC value of Basin Average in summer rises from 0.48 in Period I to 0.68 in Period II, and finally reaches 0.85 in Period III. For random error and bias there are the largest values of ME and RMSE in summer months because both the amount and frequency of precipitation are highest in this season. By analyzing all values of ME, RMSE, and BIAS for different seasons throughout the three different periods, we can conclude that the errors in Period III found in the daily and monthly comparisons (Figures 3 and 6) are primarily attributed to the overestimation of the 3B42RT-Version6 algorithm for summer rainstorms. In addition, it is worth noting that the largest relative biases occur in winter in estimating the water equivalent with snowing events. After excluding these snowing days, we found that the CC evidently increased from Period I to III, meanwhile ME, RMSE, and BIAS improved significantly in winter. Moreover, the detection of precipitating events also performs slightly better for rainy days. In general, approximately 45% of the total annual errors come from heavy rainfall events in summer, while the proportion during winter is only 15%.

[14] To help developers diagnose the impact of snow on TMPA estimates in high-latitude basins, we calculated the number of snowing days, cumulative snow water equivalent, and four representative statistical indices (i.e., CC, ME, RMSE, and BIAS) of TMPA-RT and TMPA-V6 versus Gauge for the winters from 2005 to 2010 in the Laohahe basin (see Table 3). It is notable that TMPA-RT has relatively better cool season performance during the years with the least number of snowing days. For example, the best performance occurred in the winter of 2009, which only has two snowing days and 2.35 mm of snowmelt for the whole basin. In contrast, the worst performance is found in the winter of 2010 with the maximum of snowing days (5 days) and water-equivalent cumulative snowmelt (10.54 mm). The overestimation with TMPA-RT during winter months in the Laohahe basin was especially remarkable and consistent, which might be attributed to two major reasons: (1) The IR-based retrievals with high space-time coverage, but poor correlation with rainfall (or snow water equivalent), are the main inputs of the TMPA system in high-latitude areas. Unfortunately, IR-based estimates with warm-top stratiform cloud systems perform rather poorly during the cold seasons [*Vicente et al.*, 1998; *Tian et al.*, 2007]. (2) As another confounding factor, the snow cover in winter very likely interferes with the PMW-based retrievals [*Grody*, 1991; *Ferraro et al.*, 1998], such as these two important microwave sensors of AMSR-E and AMSU-B that can cover higher-latitude bands (beyond 40°N-S). In particular, the high frequency channels (89 and 150-GHz) of AMSU-B might detect more scattering associated with precipitation sized ice particles in the winter atmosphere, which indirectly raises its retrieval precipitation rate [*Vila et al.*, 2007]. Thus, the available PMW-based calibrations of IR and the PMW data themselves covering high-latitude regions

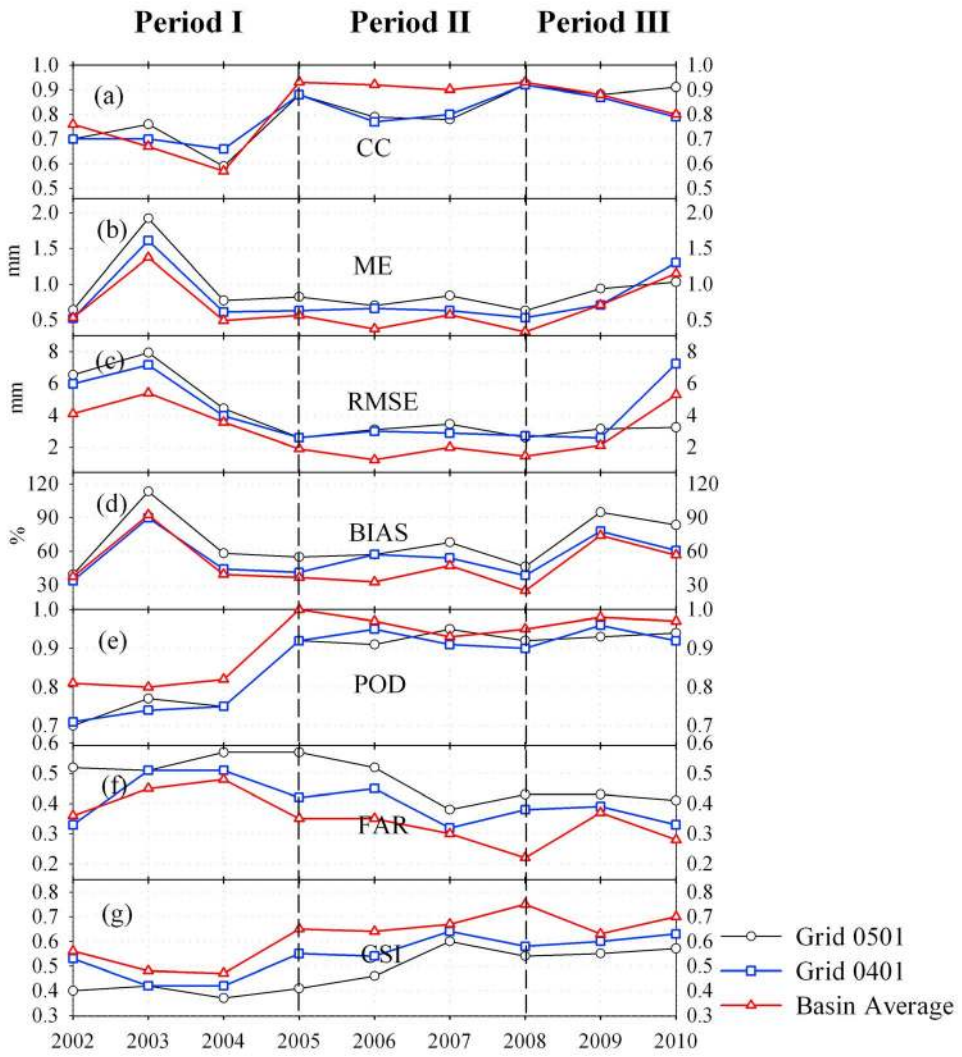

Figure 7. Annual variations of statistical indices for daily TMPA-RT versus TMPA-V6 over Grid 0501, Grid 0401, and Basin Average, respectively.

cannot offer accurate retrievals with snow events. As a result, the TMPA estimates suffer serious bias during the cool seasons.

3.4. Detection of Similarity Between TMPA-RT and TMPA-V6

[15] Some previous studies have verified that TMPA-V6 showed better performance in hydrologic simulation than TMPA-RT in many basins over the globe [*Su et al.*, 2008; *Stisen and Sandholt*, 2010; *Yong et al.*, 2010; *Bitew and Gebremichael*, 2011]. Meanwhile, the TMPA producers also suggested that the real-time data sets were made to be similar to the research products as much as possible. Therefore, we specifically address the following question that naturally arises among data users: Did the latest upgrades make TMPA-RT closer to TMPA-V6 than before? To address this issue, we first plotted the annual statistical indices of TMPA-RT versus TMPA-V6 over Grid0501, Grid0401, and Basin Average during 2002–2010 (Figure 7). The results of annual statistics show that the TMPA-RT estimates after 2005 generally have higher correlation, lower errors, and better rain detection against TMPA-V6 than before. However, TMPA-RT of Period III doesn't continue the tendency of approaching the skill of TMPA-V6 like that from Period I to Period II. Four statistics (i.e., CC, POD, FAR, and CSI) of Period III show no clear significant improvements compared with Period II. The indices of error and bias (i.e., ME, RMSE, and BIAS) are even larger than those of Period II.

[16] Considering the strong seasonality within satellite-based precipitation estimates, we further investigated the seasonal statistics of TMPA-RT versus TMPA-V6 for more insightful understanding. Figures 8a and 8c show that there are gradually increasing CC, POD, and CSI between TMPA-RT and TMPA-V6 from Period I to III during the spring and autumn seasons. Interestingly, the values of error and bias (ME, RMSE, and BIAS) and false alarm ratio (FAR) have a significant decreasing tendency for these two seasons, which is different from the annual statistics. However, such variations expected by the TMPA producers were not found

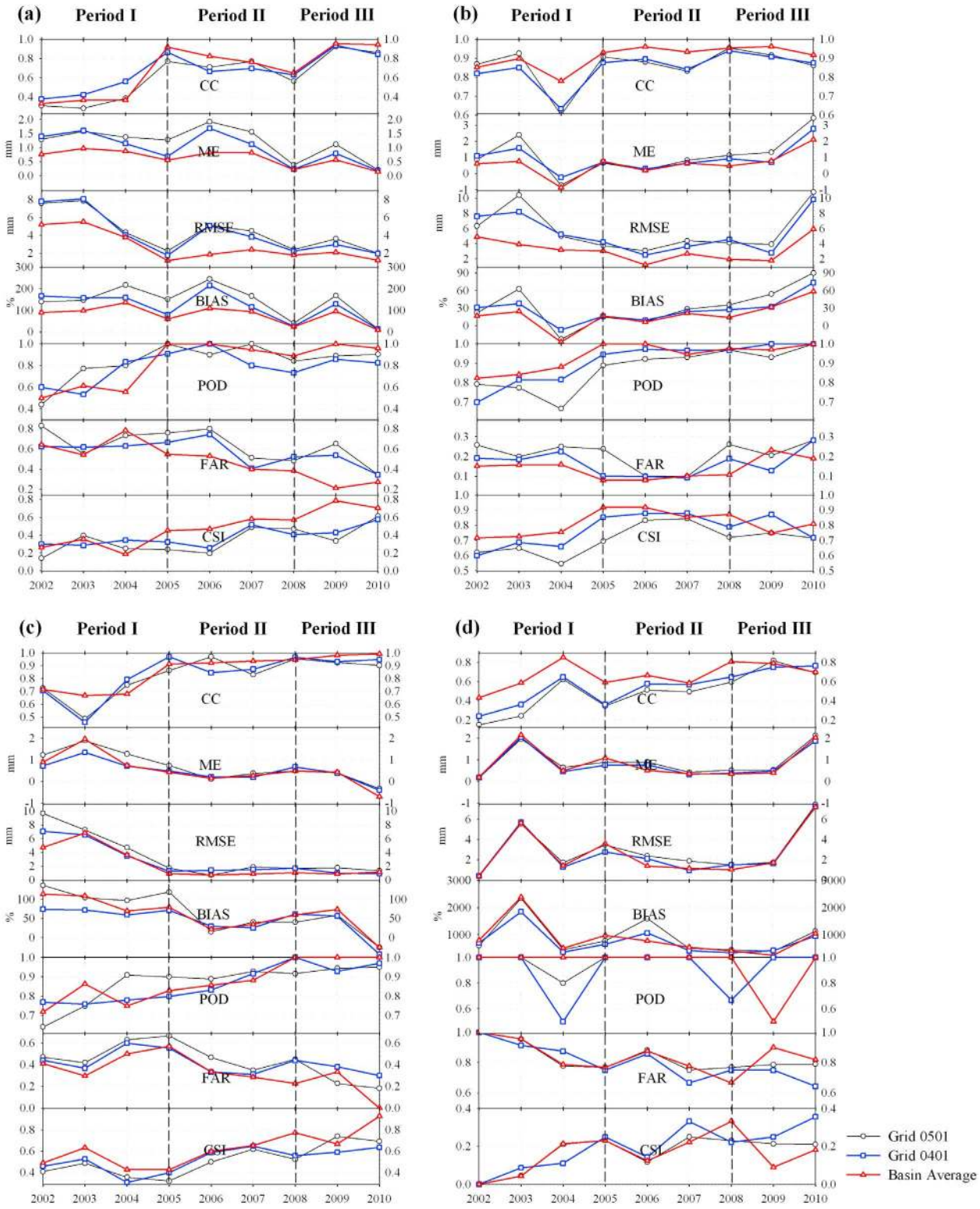

Figure 8. Same as Figure 7 but for seasonal statistics: (a) Spring [March–May (MAM)], (b) Summer [June–August (JJA)], (c) Autumn [September–November (SON)], (d) Winter [December–February (DJF)].

in the seasons of summer and winter (Figures 8b and 8d). For instance, the values of ME, RMSE, and BIAS in Period III are higher than those values in Period II during the summer months. For winter, besides similar overestimation of error and bias, the POD values of three domains even show anomalous fluctuations. Therefore, it can be concluded that relative to the prior two periods, the larger bias and error between TMPA-RT and TMPA-V6 during Period III are

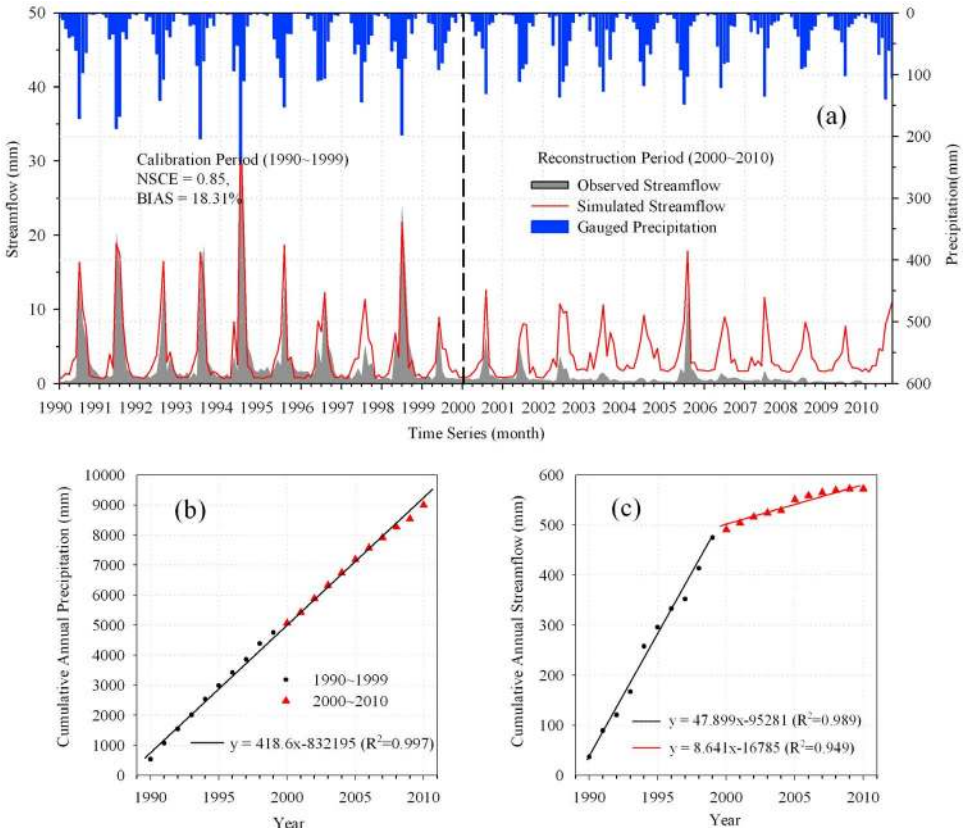

Figure 9. (a) Observed and gauge-driven VIC-simulated monthly streamflow for calibration period (1990–1999) and reconstruction period (2000–2010). (b) Cumulative annual precipitation from 1990 to 2010 for the Laohahe basin. (c) Same as Figure 9b but for streamflow.

chiefly attributed to the remarkable overestimation of the TMPA-RT algorithm for the summer rainstorms and the winter snowfall over our high-latitude basin.

4. Evaluation and Comparison of Hydrologic Streamflow Simulations

[17] Up to this point, we have directly evaluated the precipitation estimates from TMPA-RT and TMPA-V6. The purpose of this section is to assess the impacts of the TMPA-RT's upgrades over the three evolving periods from the hydrologic perspective after applying the estimates as forcing to the VIC-3L hydrologic model. The VIC-3L model was calibrated using monthly rain gauge and streamflow observations on the Laohahe basin for the period 1990–1999 by *Yong et al.* [2010]. Figure 9a shows the monthly series of observed and VIC-simulated streamflow using rain gauge inputs from 1990 to 2010. The plots of cumulative annual precipitation and streamflow indicate that the annual rainfall of the Laohahe basin hardly changed during the last twenty years (Figure 9b). However, there is a dramatic decreasing tendency with the observed discharge after 2000 (Figure 9c). *Yong et al.* [2010] concluded that human activities such as increased water diversions for irrigation, newly built reservoirs and dams, rapid development of water-consuming industries, and growth of local economies have substantially altered the natural hydrologic system. Here, we emphasize that the streamflow after 2000 cannot be used as a standard reference for assessing TMPA's hydrologic potential provided that the model parameters were estimated prior to 2000 due to the tremendous human impacts in this basin. Therefore, as recommended by some previous studies [e.g., *Wang et al.*, 2010; *Yong et al.*, 2010], we adopted the streamflow reconstructed with gauge-observed precipitation input to the hydrologic model as the surrogate for the observed streamflow during 2000–2010 (i.e., reconstruction period) in following hydrologic evaluations.

[18] We designed three simulation schemes (i.e., validation, bias-correction, and recalibration) to assess and intercompare the hydrologic potential of TMPA-RT over the three evolving periods using the reconstructed streamflow as the reference. First, we kept the same calibrated parameters optimized during the calibration period 1990–1999 unchanged and used the $\frac{1}{16}^\circ \times \frac{1}{16}^\circ$ gridded TMPA-RT and TMPA-V6 data to directly force the VIC-3L model for hydrologic simulation. Figure 10 shows that simulations using TMPA-RT significantly overestimates streamflow in the Laohahe basin mostly due to its unrealistically high precipitation estimates as presented in section 3. However, it is worth noting that there is a gradually increasing tendency in the correlation between TMPA-RT-derived and reconstructed streamflow during the three periods. For example, CC of daily streamflow in Period I is 0.02, while this value rises to 0.24 in Period II and to 0.45 in Period III.

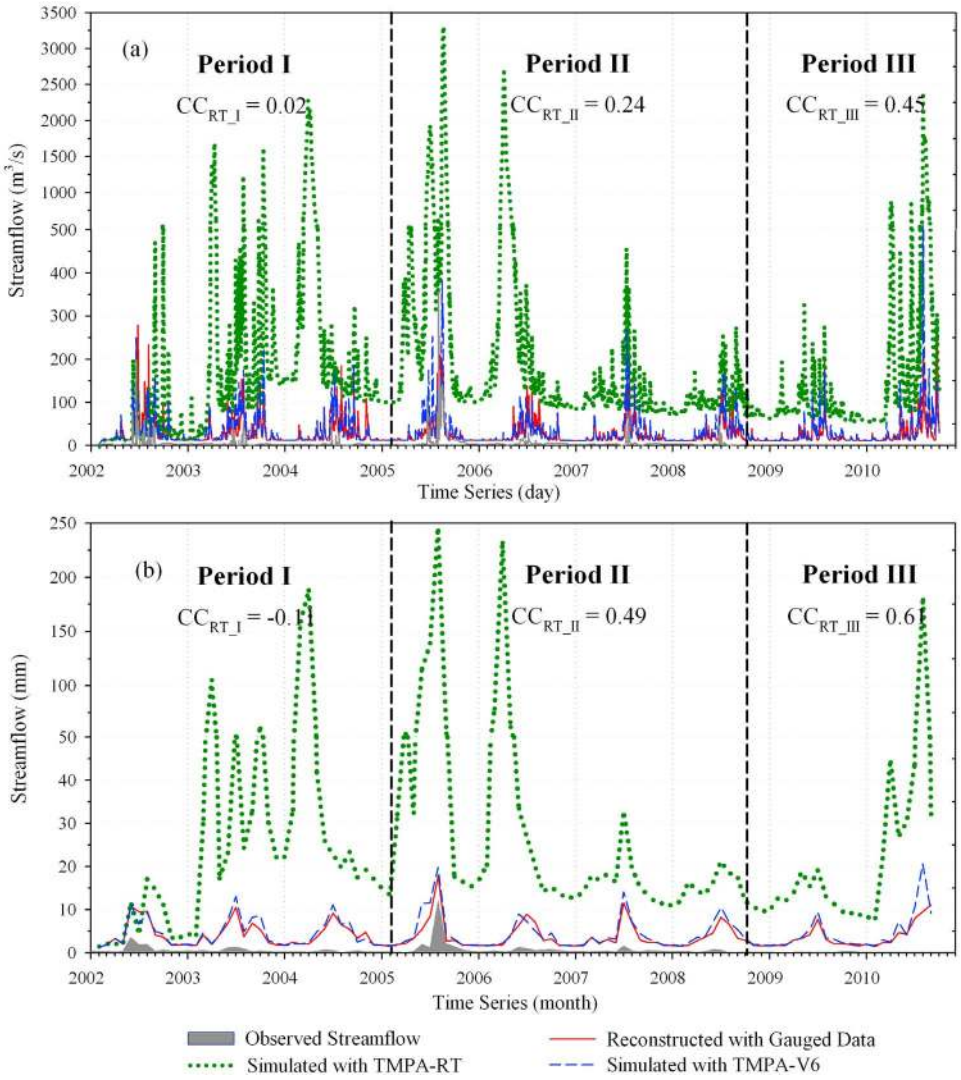

Figure 10. Hydrologic simulation scheme 1: validation for TMPA-RT and TMPA-V6. VIC-3L reconstructed streamflow with the observed gauge precipitation and VIC-3L simulated streamflow directly forced by TMPA-RT and TMPA-V6 during three evolving periods: (a) daily scale and (b) monthly scale.

With respect to monthly simulation, the values of CC are −0.11, 0.49, and 0.61 for the three periods, respectively. On the other hand, TMPA-V6 exhibits very good performance in simulating the daily and monthly variations of reconstructed streamflow, compared with TMPA-RT. Moreover, the streamflow driven by TMPA-V6 even agrees with the reconstructed reference runoff more than the observed streamflow due to the significance of land use changes and human infrastructure impacts on streamflow in the Laohahe basin. In other words, satellite-derived precipitation estimates should have greater potential applications in simulating natural hydrologic processes for typical ungauged basins which experience much lower human impacts.

[19] The hydrologic validation in Figure 10 suggests that there exists a high system bias in the TMPA-RT estimates for our study basin. We speculate that similar results might be prevailing with other high-latitude basins. Therefore, next we adopted a simple bias reduction method to potentially improve streamflow prediction using TMPA-RT at basin scale. In the proposed approach, we defined a ratio bias correction factor (*rr*) as:

$$rr = \frac{1}{1 + \mathrm{BIAS}} \tag{1}$$

where the relative bias (BIAS) is defined as following:

$$\mathrm{BIAS} = \frac{\sum_{i=1}^{n}(S_i - G_i)}{\sum_{i=1}^{n} G_i} \times 100\% \tag{2}$$

In (2), S_i is the daily or monthly precipitation of TMPA-RT at the ith time step, G_i is the corresponding gauge precipitation, and n is the number of time steps.

[20] Next, the bias correction factor (*rr*) was applied to the satellite precipitation retrievals (i.e.,*rr* × TMPA) for each of the three tested periods (*rr* was 0.5622 for Period I, 0.6038 for Period II, and 0.4918 for Period III). We kept the

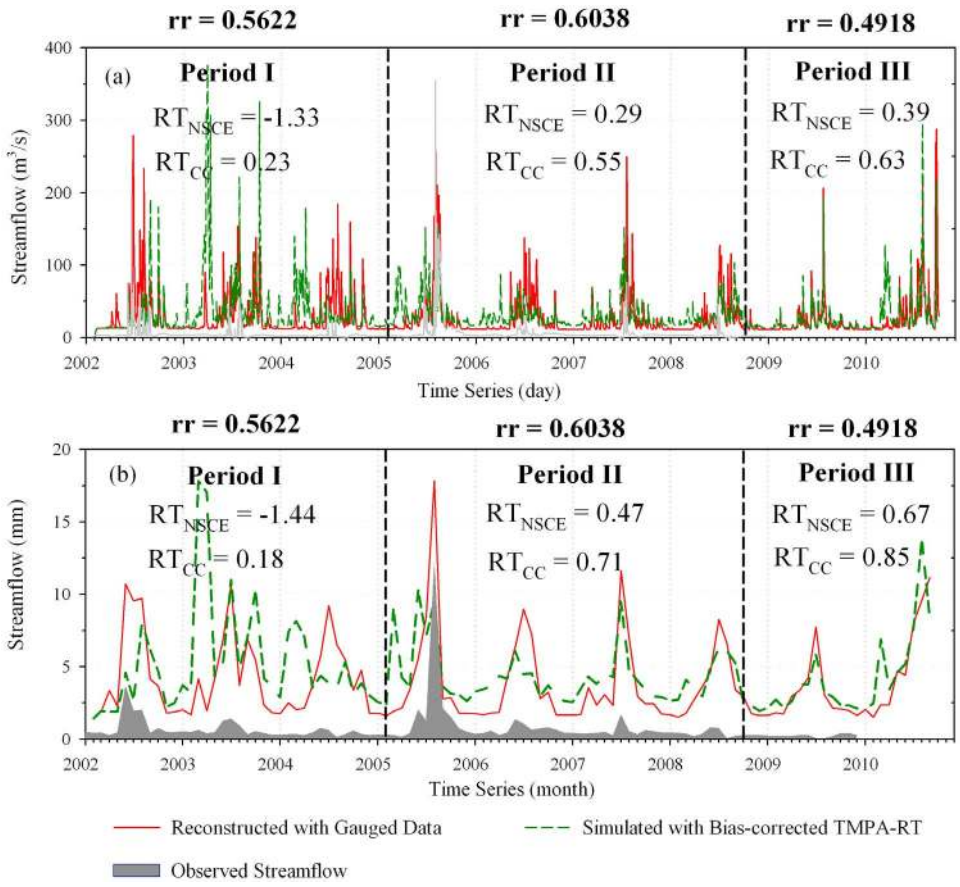

Figure 11. Hydrologic simulation scheme 2: Simulation forced with bias-adjusted TMPA-RT. Simulated streamflow with bias-adjusted TMPA-RT referenced by the reconstructed streamflow with the gauged precipitation during three evolving periods: (a) daily scale and (b) monthly scale.

calibrated model parameters the same and merely replaced the original TMPA-RT estimates with the bias-corrected inputs to drive the VIC-3L hydrologic model. As we anticipated, the simple approach of bias-correction remarkably improved the application of TMPA-RT estimates to streamflow simulation (Figure 11). The TMPA-RT-driven simulation agrees well with the reconstructed streamflow especially after 2005. The best hydrological performance was found in Period III (NSCE of 0.39 and 0.67, CC of 0.63 and 0.85 for daily and monthly streamflow prediction, respectively) despite some overestimates during the summer and winter months of 2010. Apparently, it was the higher CC and better rainfall detection skill (POD, FAR, and CSI) of TMPA-RT precipitation with rain gauges during Period III compared to the prior two periods that drastically improved its hydrologic capability. Following the simple procedure of bias-correction, the TMPA-RT was closer to observed precipitation and its potential for capturing the hydrological features of the basin was significantly enhanced for our study basin, though it still cannot achieve the simulation accuracy as in medium- or low-latitude basins (e.g., those reported by *Behrangi et al.* [2011], *Bitew and Gebremichael* [2011], and *Su et al.* [2011]).

[21] Presently, there is an increasing realization that many hydrologic models are sensitive to the meteorological forcing data, in particular precipitation [*Wilk et al.*, 2006]. If the error characteristics of input precipitation change dramatically, then it is likely that sensitive model parameters, such as soil infiltration parameters and base flow parameters will need to change accordingly in order to achieve accurate streamflow simulations [*Su et al.*, 2005; *Yong et al.*, 2010]. Although bias correction to the forcing data is the preferred approach, these error characteristics may only be known after a given algorithm was implemented and evaluated after a significant passage of time. In other words, the identification of bias may not be readily available for a recently implemented precipitation algorithm or in locations where there are scarce or nonexistent gauge networks. In the third experiment, we recalibrated the sensitive parameters of VIC-3L for the whole period of February 2002–September 2010 by using the original TMPA-RT precipitation estimates as forcing data. Table 4 lists the calibrated and recalibrated values of the seven sensitive parameters in the VIC-3L model. These parameters are briefly depicted as follows: (1) the infiltration parameter (b) which controls the amount of water that can infiltrate into the soil; (2) the three soil layer thicknesses (d_1, d_2, d_3) which affect the maximum storage available in the soil layers and consequently the water available for transpiration; (3) three base flow parameters including the maximum velocity of base flow (D_m), the fraction of maximum base flow (D_s), and the fraction of maximum soil moisture (W_s), which jointly determine how

Table 4. Comparison of Calibrated and Recalibrated Parameter Values in VIC-3L Hydrologic Model for TMPA-RT-Driven Streamflow Simulations[a]

Parameter	Unit	Typical Range	Calibrated Values With Gauge Precipitation	Recalibrated Values for TMPA-RT
b	N/A	$0 \sim 0.5$	0.01	0.0055
d_2	m	$0.1 \sim 2.0$	1.2	5.7
D_s	Fraction	$0 \sim 1.0$	0.004	0.0025
D_m	mm/day	$0 \sim 30.0$	8.0	7.3
W_s	Fraction	$0 \sim 1.0$	0.98	0.98
d_1	m	$0 \sim 0.1$	0.05	0.05
d_3	m	$0.1 \sim 2.0$	1.5	2.0

[a]Notation: In this study, the calibration period is Jan. 1990–Dec. 1999 and the recalibration period is Feb. 2002–Sep. 2010.

quickly the water stored in the third layer is withdrawn [*Liang et al.*, 1996; *Su et al.*, 2005]. Among them, the most intensive parameters are the infiltration parameter (b) and the second soil layer thicknesses (d_2), which were targeted for intensive calibration/recalibration. Similar to Figure 11, the recalibrated simulations also show that the TMPA-RT after 2005 performed much better than prior periods for hydrologic simulation (see Figure 12). From the values of NSCE and CC, it can be seen that the best performance still occurred in Period III. The recalibrated results suggest again that hydrologic potential of TMPA-RT tends to gradually increase during its three evolving periods. However, the recalibration approach compromised the model's parameterized representation of real-world physical processes. For example, the recalibrated parameter, b, is 0.0055 (see Table 4), which almost reaches its minimum value of zero. The other sensitive parameter, d_2, has an optimized value of 5.7 m that substantially exceeded the upper limit of its normal physical range (0.1–2.0 m). Thus, it can be seen that the bias of TMPA-RT overestimation was mitigated at the cost of comprising the physical representativeness of hydraulic properties of the basin, which seriously alters the basin response under varying wetness conditions. Although the recalibration may not be a physically consistent approach for modeling the hydrologic response of real basins, it certainly helps us to confirm two facts: (1) the errors in simulating streamflow forced by TMPA-RT are mostly due to the unrealistically high precipitation estimation, and (2) there is an increasing hydrologic potential for TMPA-RT in streamflow simulations over its three historic development periods. However, we did not intend to advocate the recalibration as the norm for the satellite QPE-hydrology community, rather than an investigation tactic in this study.

[22] *Hossain and Lettenmaier* [2006] have argued that a shift in paradigm is needed to properly assess estimates of rainfall from satellite sensors for modeling dynamic hydrologic processes such as the rainfall-runoff transformation and associated energy and moisture fluxes. To better understand how error characteristics of input precipitation affect hydrologic model results, we compared the error

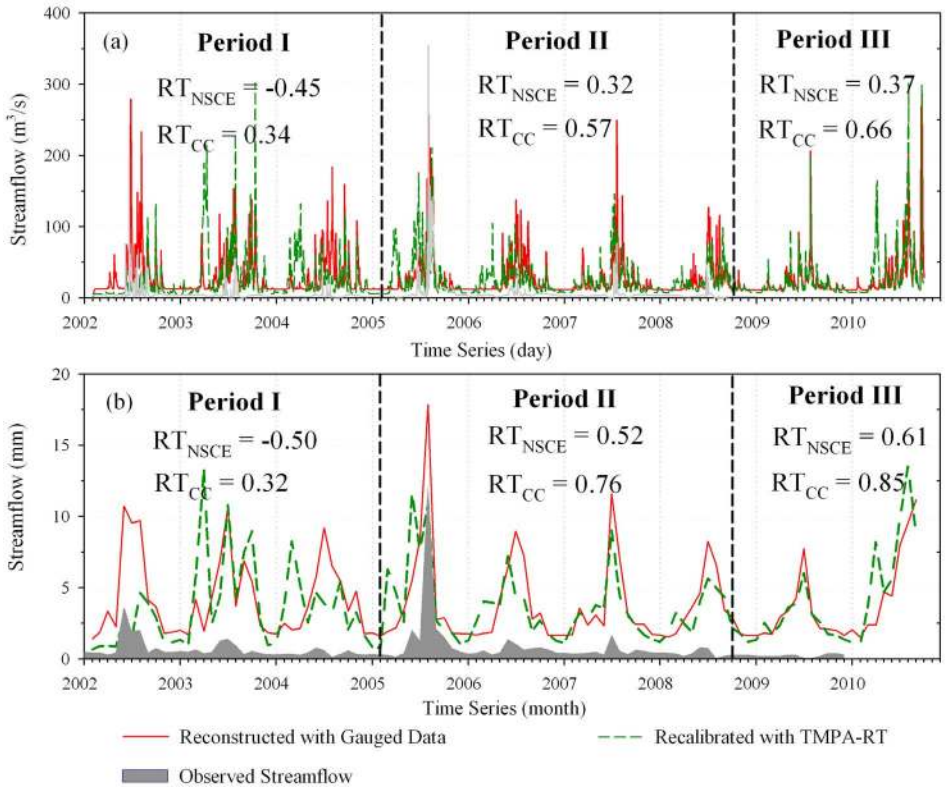

Figure 12. Hydrologic simulation scheme 3: recalibration for TMPA-RT. Recalibrated streamflow with TMPA-RT (recalibrated model parameter values listed in Table 4) referenced by the reconstructed streamflow with the gauged precipitation during three evolving periods: (a) daily scale and (b) monthly scale.

Table 5. Comparison Results of Rainfall-Runoff Error Propagation for Three Simulation Schemes, i.e., Validation, Bias-Correction, and Recalibration Through VIC-3L Hydrologic Model at Daily and Monthly Scales, Respectively

		Daily Scale						Monthly Scale					
		Period I		Period II		Period III		Period I		Period II		Period III	
Item	Index	Rainfall	Streamflow	Rainfall	Streamflow	Rainfall	Streamflow	Rainfall	Streamflow	Rainfall	Streamflow	Rainfall	Streamflow
Scheme 1: Validation	NSCE	−1.14	−161.62	0.01	−275.78	−2.05	−94.29	−0.35	−298.74	0.03	−348.21	−0.91	−205.08
	CC	0.46	0.02	0.70	0.24	0.75	0.45	0.67	−0.11	0.80	0.49	0.91	0.61
	BIAS (%)	77.86	609.95	65.61	853.20	103.34	565.77	77.86	609.79	65.46	853.45	103.57	565.62
	RMSE(mm)	5.29	385.27	3.10	482.12	4.72	298.07	46.95	48.09	30.19	59.90	51.50	38.33
Scheme 2: Bias-correction	NSCE	0.02	−1.33	0.48	0.29	0.59	0.39	0.44	−1.44	0.62	0.47	0.79	0.67
	CC	0.46	0.23	0.70	0.55	0.75	0.63	0.67	0.18	0.80	0.71	0.91	0.85
	BIAS (%)	0.00	23.78	0.00	13.60	0.00	5.75	0.00	23.76	0.00	13.60	0.00	5.78
	RMSE(mm)	3.57	46.05	2.26	22.93	1.92	25.14	30.18	4.34	23.04	2.34	18.30	1.53
Scheme 3: Recalibration	NSCE	−1.14	−0.45	0.01	0.32	−2.05	0.37	−0.35	−0.50	0.03	0.52	−0.91	0.61
	CC	0.46	0.34	0.70	0.57	0.75	0.66	0.67	0.32	0.80	0.76	0.91	0.85
	BIAS (%)	77.86	−14.66	65.61	−6.30	103.34	7.52	77.86	−14.62	65.46	−6.33	103.57	7.58
	RMSE(mm)	5.29	36.38	3.10	22.72	4.72	25.67	46.95	3.40	30.19	2.08	51.50	1.67

propagation of TMPA-RT through VIC-3L rainfall-runoff processes at daily and monthly scale for the above three types of simulation schemes. For NSCE and CC, Table 5 shows that the hydrological simulations of scheme 2 (bias-correction) and 3 (recalibration) performed much better than those of scheme 1 (validation). This suggests that both bias-correction and model-parameter adjustment can effectively remove the system bias of TMPA-RT through the VIC-3L model and then improve the hydrologic potential of satellite precipitation in this specific basin. NSCE and CC of TMPA-RT-driven streamflow in scheme 2 and 3 exhibit an apparent upward trend over the three tested periods (e.g., NSCE of −1.44, 0.47, and 0.67; CC of 0.18, 0.71, and 0.85 for the monthly streamflow simulation in scheme 2, respectively), which is closely corresponding to the trend in CC between satellite precipitation inputs and observations (e.g., CC of 0.67, 0.80, and 0.91 for the monthly rainfall in scheme 2). Among the three tested periods, the best performance is in Period III. This implies that the upgraded algorithm using climatological monthly calibration that increased the CC, POD, CSI and decreased the FAR between satellite precipitation and gauged observations potentially improved the hydrologic application of TMPA-RT. In terms of BIAS and RMSE, it is shown that the VIC-3L model significantly amplified the errors propagated from original satellite rainfall to the TMPA-RT-driven simulations (refer to the statistics of scheme 1 in Table 5). However, following precipitation bias-correction or model-parameter adjustment, both procedures having the same effect on hydrologic simulation, this situation was remarkably improved. Overall, the results of rainfall-runoff error propagation suggest that the hydrological potential of TMPA-RT tends to become better and better during its evolving periods even in high-latitude regions. The authors argue that such improvements of hydrologic prediction are closely related to the inclusion of new satellite data sources and upgrades to the precipitation algorithms in the TMPA real-time precipitation systems. Additionally, the error in rainfall versus error in runoff presented in Table 5 indicates that the hydrologic propagation of satellite rainfall error through the VIC model exhibits a quasi-linear behavior due to the large basin scale (18,112 km^2) and longer time scales (daily or monthly) in this study. While previous studies [*Nikolopoulos et al.*, 2010; *Serpetzoglou et al.*, 2010] have indicated that a strong nonlinearity exists in the rainfall-runoff error transformation, those results are generally for hourly flood simulations on smaller-scale basins (<600 km^2). Clearly, our results demonstrate that there is a dependence of satellite rainfall error propagation on basin scale.

5. Conclusions and Recommendations

[23] In this study, we have evaluated and inter-compared the TMPA-RT precipitation estimates over three major evolution periods at daily, monthly and seasonal time scales using an independent, high-quality rain gauge network in a high-latitude basin in China. Then, we investigated whether the latest updates within Period III made the TMPA-RT data more similar to the gauge-adjusted TMPA-V6 estimates as intended by the algorithm developers. Last, we designed three types of streamflow simulation experiments using the VIC-3L model forced by TMPA-RT precipitation estimates

in order to explore their hydrologic potential throughout the three evaluation periods. Results drawn from the above analyses may be specific to the Laohahe basin but are likely to be more generally applicable to basins situated in 40°–50° latitude bands; they are summarized as follows:

[24] 1. TMPA-RT estimates were least accurate and had the poorest hydrologic performance prior to February 2005 (in Period I), while substantial improvements by use of AMSR-E and AMSU-B data occurred thereafter as the developers have documented. Our results support their recommendation that users of TMPA precipitation should not utilize the real-time data sets before February 2005 for application to or feasibility studies involving hydrologic prediction or other natural hazard studies (e.g., landslides). The post-real-time research products (i.e., TMPA-V6) can be regarded as a reliable substitute to use prior to February 2005.

[25] 2. Compared to the two prior periods before October 2008 (Periods I and II), the most recent version of TMPA-RT (i.e., 3B42RT-Version6 for Period III in this study) has higher CC, POD, and CSI and lower FAR compared to rain gauge observations. However, it was noted that it also has larger ME, RMSE and BIAS in our study basin. This implied that the latest algorithm upgrades to TMPA-RT tended to increase its correlation with independent rain gauge observations and improve the skill of detecting rainy events, but was not capable of systematically reducing bias. Therefore, caution must be exercised when using the current version 6 of TMPA-RT as inputs for flood forecasting models due to its propensity to overestimate precipitation in higher-latitude basins.

[26] 3. The latest upgrades to TMPA-RT during Period III made it more statistically similar to TMPA-V6 than the real-time algorithm running in Period II during the spring and autumn seasons. However, such improved performance anticipated by both the TMPA produced and data users was not found in the summer and winter seasons due to the remarkable overestimation of the current 3B42RT-Version6 algorithm in detecting the summer rainstorms and the winter snowfall over this high-latitude basin.

[27] 4. In the present version of TMPA-RT, one of the most serious issues was its notably poor performance (i.e., BIAS > 1000%) during winter months, in particular with snowy events. Apparently, satellite-based precipitation estimates in high latitudes during cold seasons still present significant challenges. Snow covered surfaces present problems for passive microwave retrievals, which are infrequent at high latitudes. It is also possible that IR-based schemes are poorly calibrated for high-latitude, cool season precipitation estimates.

[28] 5. Prior to performing a hydrologic evaluation, streamflow was reconstructed on the Laohahe basin using rain gauge inputs to the calibrated VIC-3L model. This reconstruction step was needed in order to account for the tremendous, unnatural and difficult-to-model reductions to streamflow caused by human impacts after 2000. The first experiment directly input TMPA-RT estimates to the calibrated VIC-3L model and compared simulations with the reconstructed streamflow. Not surprisingly, the TMPA-RT-driven model simulation significantly overestimated the daily and monthly hydrographs for the entire period from 2002 to 2010. The second experiment applied a mean bias correction factor to the TMPA-RT estimates for each of the three periods and evaluated them as inputs to the calibrated VIC-3L hydrologic model. In this hydrologic evaluation, the TMPA-RT data sets revealed improvements throughout the three evolving periods. The third, naive experiment incorporated no information about TMPA-RT precipitation bias, which will be the case in basins lacking rain gauge networks, and recalibrated model parameters to the uncorrected, biased TMPA-RT estimates. The hydrologic skill in this latter experiment was essentially the same as that achieved in the second experiment. This indicates the model parameters can be estimated in a manner to effectively remove precipitation bias. However, it is noted that model parameter estimation procedures require a long, multiyear data set, over which the error characteristics of precipitation might change especially following algorithm updates. Furthermore, the recalibrated parameters didn't always represent the realistic changes of hydraulic properties for real basins. Thus, it is recommended that the best procedure to increase the hydrologic use of TMPA-RT precipitation estimates is to improve their accuracy as much as possible and be cognizant of potential biases.

[29] Looking to the future, *Huffman et al.* [2010] suggested that more work is needed to extend TMPA precipitation estimates to higher latitudes and further evaluate the effectiveness of ongoing algorithm upgrades. Compared to the post-real-time research products, TMPA-RT data have attracted the attention of hydrologists who are engaging in studies of flood forecasting and landslide warning over vast regions due to the availability of the data in near-real time over most parts of the globe. We expect the results reported here will both provide the retrieval developers with some valuable references and offer hydrologic users of TMPA-RT data a better understanding of their error characteristics and potential utilization for various operational hydrological applications in high-latitude basins. In summary, this study demonstrated that there is an increasing potential in the use of TMPA-RT in hydrologic streamflow simulations over its evolving periods. But, accurate detection and estimation of precipitation during the winter months (especially for snowing events) is still a challenging task for the satellite-based precipitation estimates. We also note that the evaluation of TMPA-RT across the time history of algorithm development presented herein potentially mixes effects due to varying storm or snowfall characteristics during various years and the changes in the retrieval algorithms themselves. Therefore, a more fair comparison could be accomplished by applying the different algorithmic versions on the same data period, a topic inviting future research. Additionally, the results shown in this study are only from a representative, semi-arid, high-latitude basin in China, so future work should extend to different hydroclimatic basins located in different latitude bands. Moreover, the evaluation framework developed herein can apply to new satellite precipitation products such as the forthcoming 3B42RT Version 7 data sets and future GPM-era products.

Appendix A: Major Upgrades of TMPA-RT During Its Three Evolving Periods

A1. Period I: 29 January 2002 to 3 February 2005

[30] Only the observations from two multichannel passive microwave radiometers, i.e., the TRMM Microwave Imager (TMI) and the Special Sensor Microwave/Imager (SSM/I)

on Defense Meteorological Satellite Program (DMSP) platforms, are converted to the merged microwave (3B40RT, or HQ product) precipitation estimates with sensor-specific versions of the Goddard Profiling Algorithm [GPROF; *Kummerow et al.*, 1996; *Olson et al.*, 1999]. During this initial period, the microwave HQ product, merged from TMI, PR (precipitation radar, TRMM product 2B31) and SSM/I, was used to calibrate the IR inputs collected from a variety of sensors flying on several geosynchronous Meteorological satellites (refer to the note of Table 1).

A2. Period II: 3 February 2005 to 1 October 2008

[31] Several important upgrades occurred at the beginning of this period for improving the data accuracy and algorithm stability of TMPA. First, Advanced Microwave Scanning Radiometer for Earth Observing System (AMSR-E) on Aqua and 3 Advanced Microwave Sounding Unit-B (AMSU-B) sensors onboard NOAA-series satellites were included into the PMW mosaics to further calibrate the TMPA-RT algorithm, which nearly doubles the typical combined microwave coverage in the latitude band 50°N-S from ~45% to nearly 80% [*Huffman et al.*, 2007]. The polar orbits of AMSR-E and AMSU-B provide broader nominal coverage (see Table 1). Especially, the use of AMSU-B offers an excellent opportunity to reduce the errors associated with the inadequate samples by combining PMW information from three NOAA POES satellites spaced approximately 4 h apart with a spatial resolution of 16 km at nadir and a wider swath than prior SSMI (2200 km) [*Vila et al.*, 2007]. However, both AMSU-B and AMSR-E still have some limitations in their retrieval techniques which prevent useful precipitation estimates over many land surfaces or sea ice. Second, the Microwave Humidity Sounder (MHS) on NOAA-18 was incorporated in TMPA-RT to replace the AMSU-B on board NOAA-17 since 27 November 2007. Similar to AMSU-B, the MHS contains 5 channels and maintains almost same algorithm-wise within TMPA-RT. But it was an afternoon sounder with a 1330 equator-crossing time, while the previous AMSU-B on NOAA-17 has a morning equator-crossing time of around 1030 local time [*Labow et al.*, 2011]. According to *Turk et al.* [2010], the local crossing time of the AMSU-like sounders did have an impact upon the soil moisture simulated with two land surface models. So presumably they might also affect the hydrologic performance of the TRMM-based precipitation estimation. Third, inter-satellite calibration in the HQ product is climatological, which reduced the real-time computational load and prepared for the eventual decommissioning of TRMM. Finally, the microwave-calibrated IR coefficients are recomputed every three hr to better control unrealistically high estimates associated to unusually cold IR background temperatures (Tb's) but with low rainfall rates, such as with high-level cirrus clouds (ftp://trmmopen.gsfc.nasa.gov/pub/merged/3B4XRT_doc.pdf).

A3. Period III: 1 October 2008 to Present

[32] The last major upgrades for the TMPA real-time system occurred on 17 February 2009. The data sets of the new Version 6 of the TMPA-RT (hereafter "3B42RT-Version6"; note that this should not to be confused with TMPA post-real time product "3B42V6") starting from 1 October 2008 were released so as to provide the users a backlog for validation and application activities with the new data. Once the new system is stable, the algorithm developers will seriously consider that the entire data record of TMPA-RT might be reprocessed by the 3B42RT-Version6 scheme. The primary goal of the new design of this algorithm and input data is to enable the real-time TMPA-RT and the post real-time gauge-adjusted products TMPA-V6 systems to be as similar as possible for ensuring consistency between these two data sets [*Huffman et al.*, 2010]. One important difference between them is the calibrator of TMPA-V6, TRMM Combined Instrument (TCI) that combines data from both TMI and PR, is not available in real time. Therefore, the developers first determined a matched histogram calibration of TMI to the TCI, computed from 10 years of coincident data to establish the climatology for each calendar month. Then, a climatological monthly calibration of TCI to 3B43 V6 (another TRMM product computed at monthly time intervals; not to be confused with aforementioned "3B42V6" and "3B42RT-Version6") is calculated as a simple ratio on a $1° \times 1°$ grid, aggregated to an overlapping $3° \times 3°$ template, and using 10 years of data. Finally, the TMI-TCI and TCI-3B43 calibrations are successively applied to the preliminary real-time products to create the 3B42RT-Version 6 products. One of the main purposes of this algorithm upgrade is to reduce the bias of TMPA-RT over land. In addition, the AMSU-B sensor on NOAA-17 was inactive on 12 December 2009 and it was replaced by the MHS sensor on the European Operational Meteorological (MetOp) satellite since 27 March 2009 (Table 1). Later enhancements to the TMPA standard products mainly include improving error quantification and more importantly, extension to higher latitudes.

[33] **Acknowledgments.** This work was financially supported by the Major Program of National Natural Science Foundation of China (51190090) and the 111 Project (B08048). Also this work is partially sponsored by the National Science Foundation for Young Scientists of China (40901017), the Open Fund of State Key Laboratory of Hydroscience and Engineering (sklhse-2011-A-01), and the Innovative Research Team and Independent Innovation Project of State Key Laboratory of Hydrology-Water Resources and Hydraulic Engineering (2009585412, 2009586512). The first author acknowledges the computational facility provided by Hydrometeorology and Remote Sensing Laboratory and Atmospheric Radar Research Center at University of Oklahoma Research Campus. Additionally, the authors would like to thank three anonymous reviewers who helped to improve the earlier version of this paper. Last but not least, we wish to extend our appreciation to the helpful suggestions of Fengge Su and Jiahu Wang for the use of VIC-3L model. The TMPA data used in this study were provided by the NASA/Goddard Space Flight Center's laboratory for Atmospheres and PPS, which develop and compute the TMPA as a contribution to TRMM.

References

Astin, I. (1997), A survey of studies into errors in large scale space-time averages of rainfall, cloud cover, sea surface processes and the Earth's radiation budget as derived from low orbit satellite instruments because of their incomplete temporal and spatial coverage, *Surv. Geophys.*, *18*, 385–403, doi:10.1023/A:1006512715662.

Behrangi, A., B. Khakbaz, T. C. Jaw, A. AghaKouchak, K. Hsu, and S. Sorooshian (2011), Hydrologic evaluation of satellite precipitation products over a mid-size basin, *J. Hydrol.*, *397*, 225–237, doi:10.1016/j.jhydrol.2010.11.043.

Bitew, M. M., and M. Gebremichael (2011), Evaluation of satellite rainfall products through hydrologic simulation in a fully distributed hydrologic model, *Water Resour. Res.*, *47*, W06526, doi:10.1029/2010WR009917.

Dinku, T., S. J. Connor, and P. Seccato (2010), Comparison of CMORPH and TRMM-3B42 over mountainous regions of Africa and South America Satellite, in *Applications for Surface Hydrology*, edited by F. Hossain and M. Gebremichael, pp. 193–204, Springer, New York.

Ebert, E. E., J. E. Janowiak, and C. Kidd (2007), Comparison of near-real-time precipitation estimates from satellite observations and numerical models, *Bull. Am. Meteorol. Soc.*, *88*, 47–64, doi:10.1175/BAMS-88-1-47.

Ferraro, R. R., E. A. Smith, W. Berg, and G. J. Huffman (1998), A screening methodology for passive microwave precipitation retrieval algorithms, *J. Atmos. Sci.*, *55*, 1583–1600, doi:10.1175/1520-0469(1998)055<1583:ASMFPM>2.0.CO;2.

Gottschalck, J., J. Meng, M. Rodell, and P. Houser (2005), Analysis of multiple precipitation products and preliminary assessment of their impact on global land data assimilation system land surface states, *J. Hydrometeorol.*, *6*(5), 573–598, doi:10.1175/JHM437.1.

Gourley, J. J., Y. Hong, Z. L. Flamig, L. Li, and J. Wang (2010), Intercomparison of rainfall estimates from radar, satellite, gauge, and combinations for a season of record rainfall, *J. Appl. Meteorol. Climatol.*, *49*, 437–452, doi:10.1175/2009JAMC2302.1.

Griffith, G. C., W. L. Woodley, and P. G. Grube (1978), Rain estimation from geosynchronous satellite imagery-visible and infrared studies, *Mon. Weather Rev.*, *106*, 1153–1171, doi:10.1175/1520-0493(1978)106<1153:REFGSI>2.0.CO;2.

Grody, N. C. (1991), Classification of snow cover and precipitation using the Special Sensor Microwave Imager, *J. Geophys. Res.*, *96*(D4), 7423–7435, doi:10.1029/91JD00045.

Hirpa, F. A., M. Gebremichael, and T. Hopson (2010), Evaluation of high resolution satellite precipitation products over very complex terrain in Ethiopia, *J. Appl. Meteorol. Climatol.*, *49*(5), 1044–1051, doi:10.1175/2009JAMC2298.1.

Hong, Y., K. L. Hsu, X. Gao, and S. Sorooshian (2004), Precipitation estimation from remotely sensed imagery using artificial neural network–cloud classification system (PERSIANN-CCS), *J. Appl. Meteorol. Climatol.*, *43*(12), 1834–1853, doi:10.1175/JAM2173.1.

Hong, Y., R. F. Adler, F. Hossain, S. Curtis, and G. J. Huffman (2007), A first approach to global runoff simulation using satellite rainfall estimation, *Water Resour. Res.*, *43*, W08502, doi:10.1029/2006WR005739.

Hossain, F., and D. P. Lettenmaier (2006), Flood prediction in the future: Recognizing hydrologic issues in anticipation of the Global Precipitation Measurement mission, *Water Resour. Res.*, *42*, W11301, doi:10.1029/2006WR005202.

Hou, Y. (2008), The Global Precipitation Measurement (GPM) mission: Overview and U.S. science status, paper presented at International Geoscience and Remote Sensing Symposium (IGARSS) 2008, IEEE, Boston, Mass.

Huffman, G. J., R. F. Adler, M. Morrissey, D. T. Bolvin, S. Curtis, R. Joyce, B. McGavock, and J. Susskind (2001), Global precipitation at one-degree daily resolution from multisatellite observations, *J. Hydrometeorol.*, *2*, 36–50, doi:10.1175/1525-7541(2001)002<0036:GPAODD>2.0.CO;2.

Huffman, G. J., R. F. Adler, D. T. Bolvin, G. Gu, E. J. Nelkin, K. P. Bowman, Y. Hong, E. F. Stocker, and D. B. Wolff (2007), The TRMM Multi-satellite Precipitation Analysis (TMPA): Quasi-Global, multi-year, combined-sensor precipitation estimates at fine scales, *J. Hydrometeorol.*, *8*, 38–55, doi:10.1175/JHM560.1.

Huffman, G. J., R. F. Adler, D. T. Bolvin, and E. J. Nelkin (2010), The TRMM Multi-satellite Precipitation Analysis (TMPA), in *Satellite Applications for Surface Hydrology*, edited by F. Hossain and M. Gebremichael, pp. 3–22, Springer, New York.

Joyce, R. J., J. E. Janowiak, P. A. Arkin, and P. Xie (2004), CMORPH: A method that produces global precipitation estimates from passive microwave and infrared data at high spatial and temporal resolution, *J. Hydrometeorol.*, *5*, 487–503, doi:10.1175/1525-7541(2004)005<0487:CAMTPG>2.0.CO;2.

Khan, S. I., Y. Hong, J. Wang, K. K. Yilmaz, J. J. Gourley, R. F. Adler, G. R. Brakenridge, F. Policelli, S. Habib, and D. Irwin (2011), Satellite remote sensing and hydrologic modeling for flood inundation mapping in Lake Victoria Basin: Implications for hydrologic prediction in ungauged basins, *IEEE Trans. Geosci. Remote Sens.*, *49*(1), 85–95, doi:10.1109/TGRS.2010.2057513.

Kubota, T., et al. (2007), Global precipitation map using satellite-borne microwave radiometers by the GSMaP Project: Production and validation, *IEEE Trans. Geosci. Remote Sens.*, *45*, 2259–2275, doi:10.1109/TGRS.2007.895337.

Kummerow, C., W. S. Olson, and L. Giglio (1996), A simplified scheme for obtaining precipitation and vertical hydrometeor profiles from passive microwave sensors, *IEEE Trans. Geosci. Remote Sens.*, *34*(5), 1213–1232, doi:10.1109/36.536538.

Kummerow, A., et al. (2000), The status of the Tropical Rainfall Measuring Mission (TRMM) after two years in orbit, *J. Appl. Meteorol.*, *39*, 1965–1982, doi:10.1175/1520-0450(2001)040<1965:TSOTTR>2.0.CO;2.

Labow, G. J., J. R. Herman, L.-K. Huang, S. A. Lloyd, M. T. DeLand, W. Qin, J. Mao, and D. E. Larko (2011), Diurnal variation of 340 nm Lambertian equivalent reflectivity due to clouds and aerosols over land and oceans, *J. Geophys. Res.*, *116*, D11202, doi:10.1029/2010JD014980.

Li, L., Y. Hong, J. Wang, R. F. Adler, F. S. Policelli, S. Habib, D. Irwn, T. Korme, and L. Okello (2009), Evaluation of the real-time TRMM-based multi-satellite precipitation analysis for an operational flood prediction system in Nzoia Basin, Lake Victoria, Africa, *Nat. Hazards*, *50*, 109–123, doi:10.1007/s11069-008-9324-5.

Liang, X., D. P. Lettenmaier, E. F. Wood, and S. J. Burges (1994), A simple hydrologically based model of land surface water and energy fluxes for GSMs, *J. Geophys. Res.*, *99*(D7), 14,415–14,428, doi:10.1029/94JD00483.

Liang, X., E. F. Wood, and D. P. Lettenmaier (1996), Surface soil moisture parameterization of the VIC-2L model: Evaluation and modification, *Global Planet. Change*, *13*, 195–206, doi:10.1016/0921-8181(95)00046-1.

Maddox, R. A., J. Zhang, J. J. Gourley, and K. W. Howard (2002), Weather radar coverage over the contiguous United States, *Weather Forecast.*, *17*, 927–934, doi:10.1175/1520-0434(2002)017<0927:WRCOTC>2.0.CO;2.

Margulis, S., and D. Entekhabi (2001), Temporal disaggregation of satellite-derived monthly precipitation estimates and resulting propagation of error in partitioning of water at the land surface, *Hydrol. Earth Syst. Sci.*, *5*(1), 27–38, doi:10.5194/hess-5-27-2001.

Nikolopoulos, E. I., E. N. Anagnostou, F. Hossain, M. Gebremichael, and M. Borga (2010), Understanding the scale relationships of uncertainty propagation of satellite rainfall through a distributed hydrologic model, *J. Hydrometeorol.*, *11*, 520–532, doi:10.1175/2009JHM1169.1.

Olson, W. S., C. D. Kummerow, Y. Hong, and W.-K. Tao (1999), Atmospheric latent heating distributions in the tropics derived from satellite passive microwave radiometer measurements, *J. Appl. Meteorol. Climatol.*, *38*(6), 633–664, doi:10.1175/1520-0450(1999)038<0633:ALHDIT>2.0.CO;2.

Romilly, T. G., and M. Gebremichael (2011), Evaluation of satellite rainfall estimates over Ethiopian 15 river basins, *Hydrol. Earth Syst. Sci.*, *15*, 1505–1514, doi:10.5194/hess-15-1505-2011.

Serpetzoglou, E., E. N. Anagnostou, A. Papadopoulos, E. I. Nikolopoulos, and V. Maggioni (2010), Error propagation of remote sensing rainfall estimates in soil moisture prediction from a land surface model, *J. Hydrometeorol.*, *11*, 705–720, doi:10.1175/2009JHM1166.1.

Simpson, J., R. F. Adler, and G. R. North (1988), A proposed Tropical Rainfall Measuring Mission (TRMM) satellite, *Bull. Am. Meteorol. Soc.*, *69*, 278–295, doi:10.1175/1520-0477(1988)069<0278:APTRMM>2.0.CO;2.

Simpson, J., C. Kummerow, W. K. Tao, and R. F. Adler (1996), On the Tropical Rainfall Measuring Mission (TRMM), *Meteorol. Atmos. Phys.*, *60*, 19–36, doi:10.1007/BF01029783.

Smith, E., et al. (2007), The International Global Precipitation Measurement (GPM) program and mission: An overview, in *Measuring Precipitation From Space: EURAINSAT and the Future*, *Adv. Space Res.*, vol. 28, edited by V. Levizzani and F. J. Turk, pp. 611–653, Springer, New York, doi:10.1007/978-1-4020-5835-6_48.

Sorooshian, S. (2004), Commentary-GEWEX (Global Energy and Water Cycle Experiment) at the 2004 Joint Scientific Committee Meeting, *GEWEX Newsl.*, *14*(2), 2.

Sorooshian, S., K. L. Hsu, X. Gao, H. Gupta, B. Imam, and D. Braithwaite (2000), Evaluation of PERSIANN system satellite-based estimates of tropical rainfall, *Bull. Am. Meteorol. Soc.*, *81*, 2035–2046, doi:10.1175/1520-0477(2000)081<2035:EOPSSE>2.3.CO;2.

Steiner, M., T. L. Bell, Y. Zhang, and E. F. Wood (2003), Comparison of two methods for estimating the sampling-related uncertainty of satellite rainfall averages based on a large radar dataset, *J. Clim.*, *16*, 3759–3778, doi:10.1175/1520-0442(2003)016<3759:COTMFE>2.0.CO;2.

Stisen, S., and I. Sandholt (2010), Evaluation of remote sensing based rainfall products through predictive capability in hydrological runoff modeling, *Hydrol. Processes*, *24*, 879–891, doi:10.1002/hyp.7529.

Su, F., J. C. Adam, L. C. Bowling, and D. P. Lettenmaier (2005), Streamflow simulations of the terrestrial Arctic domain, *J. Geophys. Res.*, *110*, D08112, doi:10.1029/2004JD005518.

Su, F., Y. Hong, and D. P. Lettenmaier (2008), Evaluation of TRMM Multisatellite Precipitation Analysis (TMPA) and its utility in hydrologic prediction in La Plata Basin, *J. Hydrometeorol.*, *9*(4), 622–640, doi:10.1175/2007JHM944.1.

Su, F., H. Gao, G. J. Huffman, and D. P. Lettenmaier (2011), Potential utility of the real-time TMPA-RT precipitation estimates in streamflow prediction, *J. Hydrometeorol.*, *12*, 444–455, doi:10.1175/2010JHM1353.1.

Tapiador, F. J., et al. (2012), Global precipitation measurement: Methods, datasets and applications, *Atmos. Res.*, *104–105*, 70–97, doi:10.1016/j.atmosres.2011.10.021.

Tian, Y., C. D. Peters-Lidard, B. J. Choudhury, and M. Garcia (2007), Multitemporal analysis of TRMM-based satellite precipitation products for land data assimilation applications, *J. Hydrometeorol.*, *8*, 1165–1183, doi:10.1175/2007JHM859.1.

Tobin, K. J., and M. E. Bennett (2010), Adjusting satellite precipitation data to facilitate hydrologic modeling, *J. Hydrometeorol.*, *11*(4), 966–978, doi:10.1175/2010JHM1206.1.

Turk, F. J., and S. D. Miller (2005), Toward improving estimates of remotely sensed precipitation with MODIS/AMSR-E blended data techniques, *IEEE Trans. Geosci. Remote Sens.*, *43*, 1059–1069, doi:10.1109/TGRS.2004.841627.

Turk, F. J., G. V. Mostovoy, and V. G. Anantharaj (2010), Soil moisture sensitivity to NRL-Blend high-resolution precipitation products: Analysis of simulations with two land surface models, *IEEE J. Sel. Top. Appl. Earth Obs. Remote Sens.*, *3*, 32–48, doi:10.1109/JSTARS.2009.2034024.

Vicente, G. A., R. A. Scofield, and W. P. Menzel (1998), The operational GOES infrared rainfall estimation technique, *Bull. Am. Meteorol. Soc.*, *79*, 1883–1898, doi:10.1175/1520-0477(1998)079<1883:TOGIRE>2.0.CO;2.

Vila, D., R. Ferraro, and R. Joyce (2007), Evaluation and improvement of AMSU precipitation retrievals, *J. Geophys. Res.*, *112*, D20119, doi:10.1029/2007JD008617.

Wang, J., Y. Hong, J. J. Gourley, P. Adhikari, L. Li, and F. Su (2010), Quantitative assessment of climate change and human impacts on long-term hydrologic response: A case study in a sub-basin of the Yellow River, China, *Int. J. Climatol.*, *30*, 2130–2137, doi:10.1002/joc.2023.

Wang, J., et al. (2011), The Coupled Routing and Excess STorage (CREST) distributed hydrological model, *Hydrol. Sci. J.*, *56*, 84–98, doi:10.1080/02626667.2010.543087.

Wilk, J., D. Kniveton, L. Andersson, R. Layberry, M. C. Todd, D. Hughes, S. Ringrose, and C. Vanderpost (2006), Estimating rainfall and water balance over the Okavango River Basin for hydrological application, *J. Hydrol.*, *331*, 18–29, doi:10.1016/j.jhydrol.2006.04.049.

Wu, H., R. F. Adler, Y. Hong, Y. Tian, and F. Policelli (2012), Evaluation of satellite-based real-time global flood detection and prediction with a hydrological model, *J. Hydrometeorol.*, in press.

Yong, B., L. L. Ren, Y. Hong, J. H. Wang, J. J. Gourley, S. H. Jiang, X. Chen, and W. Wang (2010), Hydrologic evaluation of Multisatellite Precipitation Analysis standard precipitation products in basins beyond its inclined latitude band: A case study in Laohahe basin, China, *Water Resour. Res.*, *46*, W07542, doi:10.1029/2009WR008965.